Oncogenic and teratogenic effects of p53^{Y217C}, a mouse model of the human hotspot mutant p53^{Y220C}

Sara Jaber[1,2,3,4,8], Eliana Eldawra[1,2,3,4,8], Jeanne Rakotopare[1,2,3,4], Marc Gabriel[2,3,4,5], Vincent Lejour[1,2,3,4], Iva Simeonova[3,4,6,7], Antonin Morillon[2,3,4,5], Boris Bardot[1,2,3,4*], and Franck Toledo[1,2,3,4*]

[1]Genetics of Tumor Suppression, Institut Curie, Paris, France; [2]CNRS UMR3244, Paris, France; [3]Sorbonne University, Paris, France; [4]PSL Research University, Paris, France; [5]Non Coding RNA, Epigenetic and Genome Fluidity, Institut Curie, Paris, France; [6]Chromatin dynamics, Institut Curie, Paris, France; [7]CNRS, UMR3664, Paris, France; [8]These authors contributed equally to this work.*correspondence : franck.toledo@curie.fr; boris.bardot@curie.fr.

Abstract

Missense "hotspot" mutations localized in six p53 codons account for 20% of *TP53* mutations in human cancers. Hotspot p53 mutants have lost the tumor suppressive functions of the wildtype protein, but whether they may gain additional functions promoting tumorigenesis remains controversial. Here we generated *Trp53*^{Y217C}, a mouse model of the human hotspot mutant *TP53*^{Y220C}. DNA damage responses were lost in p53$^{Y217C/Y217C}$ cells. Surprisingly, intercrosses from p53$^{+/Y217C}$ heterozygotes yielded only one p53$^{Y217C/Y217C}$ female for nineteen p53$^{Y217C/Y217C}$ males at weaning, a skewed distribution explained by the high frequency of p53$^{Y217C/Y217C}$ female embryos with exencephaly and the death of most p53$^{Y217C/Y217C}$ female neonates. Furthermore, parturition was impaired in pregnant p53$^{Y217C/Y217C}$ females. Finally, p53$^{Y217C/Y217C}$ males died earlier than p53$^{-/-}$ males, with more aggressive thymic lymphomas. Together, these data indicate that the p53^{Y217C} mutation not only abrogates wildtype p53 functions, but also exerts additional effects promoting oncogenesis in males and teratogenesis or dystocia in females.

Key words

hotspot p53 mutant, Y220C, gain of function, exencephaly, dystocia, sex-specific effects.

Introduction

Somatic alterations in the *TP53* gene, encoding the tumor suppressor p53, are the most common events in human tumors (Hollstein et al., 1991). The p53 protein is a stress sensor stabilized and activated in response to potentially oncogenic insults. In its tetrameric active form, wildtype (WT) p53 can trigger a transcriptional program to induce various responses including cell cycle arrest, senescence, apoptosis or metabolic changes (Beckerman and Prives, 2010). In human cancers, about 75% of all *TP53* alterations are missense mutations, and the eight most frequent ("hotspot") missense mutations (R175H, Y220C, G245S, R248Q, R248W, R273H, R273C and R282W) affect six residues localized in the p53 DNA-binding domain (DBD) and account for 20% of all *TP53* mutations (Hainaut and Pfeifer, 2016). The fact that most *TP53* mutations are missense substitutions suggested that cells expressing mutant p53 might have a selective advantage over cells lacking p53, and evidence for this was first gained by expressing various p53 mutants in p53-null cells, and observing enhanced tumorigenic potential in nude mice or increased plating efficiency in agar cell culture (Dittmer et al., 1993). Mouse models expressing hotspot p53 mutants next helped to define potential mechanisms accounting for accelerated tumorigenesis. First, a dominant-negative effect (DNE) may be observed in heterozygotes, if the mutant p53 inhibits the WT p53 protein in hetero-tetramers (Gencel-Augusto and Lozano, 2020). Evidence that this mechanism accounts for accelerated tumorigenesis was notably reported in human leukemia (Boettcher et al., 2019). A second mechanism is a gain-of-function (GOF), i.e. the acquisition by mutant p53 of new oncogenic properties (Amelio and Melino, 2020; Stein et al., 2020). Although the DNA sequence specificity of p53 mutants is impaired, leading to a loss of WT functions (LOF), many p53 mutant proteins are stabilized in the cell and might engage in aberrant interactions with other transcription factors or chromatin-modifying complexes, leading to the acquisition of GOF phenotypes (Kim and Deppert, 2007; Pfister and Prives, 2017). However, a few recent studies challenged the pathological importance of mutant p53 GOF, or at least its relevance in anti-cancer therapeutic strategies (Aubrey et al., 2018; Boettcher et al., 2019; Wang et al., 2023). An alternative hypothesis emerged, postulating that the tumorigenic properties of a p53 mutant might result from a separation-of-function (SOF), if the mutant retains pro-proliferative or pro-survival functions of WT p53 while losing its tumor suppressive activities (Kennedy and Lowe, 2022). The concept of SOF was first proposed for *TP53* exon-6 truncating mutations, which

mimic a naturally occurring alternative p53 splice variant (Shirole et al., 2016), but may apply to some p53 missense mutations, for example $p53^{R248W}$ (Humpton et al., 2018). Importantly, the analysis of various mutant p53 alleles *in vivo* appears crucial for a better understanding of their contribution to tumorigenesis, because GOF/SOF phenotypes may vary depending on the mutated residue, its specific mutation, the cellular context or genetic background (Dibra et al., 2024; Hanel et al., 2013; Kadosh et al., 2020; Kim and Lozano, 2018; Kotler et al., 2018; McCann et al., 2022; Xiong et al., 2022).

In human cancers, the *TP53*^{Y220C} mutation is the most frequent missense mutation outside of the DNA-binding surface of p53 (Hainaut and Pfeifer, 2016). The somatic *TP53*^{Y220C} mutation accounts for over 100,000 new cancer cases per year worldwide, and a germline *TP53*^{Y220C} mutation was reported in 15 families with the Li-Fraumeni syndrome (LFS) of cancer predisposition (Bouaoun et al., 2016). This mutation causes a structural change in the DBD localized at the periphery of the β–sandwich region of the protein, far from the surface contact of DNA. The mutation from a tyrosine to a cysteine markedly lowers the thermodynamic stability of the DBD, leading to a largely unfolded and inactive protein at body temperature (Joerger et al., 2006), and a molecule designed to bind $p53^{Y220C}$ and restore WT protein conformation appears as a promising anti-cancer drug (Dumbrava et al., 2022). Analyses of the impact of $p53^{Y220C}$ in cancer cell lines led to conflicting results. On one hand, overexpression of $p53^{Y220C}$ in a p53-null cell line increased its capacity for migration or invasion (Zhou et al., 2022), and a decreased expression of $p53^{Y220C}$, caused by RNA interference or various chemical compounds, promoted cell death or decreased the migratory or invasive capacities of cells (Tseng et al., 2022; Vikhanskaya et al., 2007; Zhou et al., 2022). On the other hand, the removal by CRISPR/Cas9 of p53 mutants with reported GOF - including $p53^{Y220C}$ - in diverse cancer cell lines had no significant impact on cell survival or proliferation, and the cell death caused by RNA interference against $p53^{Y220C}$ might result from non-specific toxic effects (Wang et al., 2023). Here, to gain a better understanding of the impact of the $p53^{Y220C}$ mutation *in vivo*, we generated a mouse model with a targeted *Trp53*^{Y217C} mutation - the mouse equivalent to human *TP53*^{Y220C} (Figure S1) - and analyzed animals and cells carrying one or two copies of the mutant allele.

Results

Targeting of a p53^{Y217C} mutation in the mouse

We used homologous recombination in 129/SvJ ES cells to target the p53^{Y217C} mutation at the mouse *Trp53* locus. Mice expressing p53^{Y217C} conditionally were generated by using a targeting vector containing transcriptional stops flanked by LoxP sites (LSL) upstream of coding sequences, and the p53^{Y217C} mutation in exon 6 (Figure 1A-D). p53$^{+/LSL\text{-}Y217C}$ mice were then crossed with mice carrying the PGK-Cre transgene (Lallemand et al., 1998) to excise the LSL cassette and obtain p53$^{+/Y217C}$ mice, expressing the mutant protein constitutively. After two backcrosses over a C57BL/6J background, mouse embryonic fibroblasts (MEFs) were prepared from intercrosses of p53$^{+/Y217C}$ mice (Figure 1E). We extracted RNAs from p53$^{Y217C/Y217C}$ MEFs then sequenced p53 mRNAs to verify that the p53^{Y217C} coding sequence was identical to the wildtype p53 (p53^{WT}) sequence, except for the desired missense mutation and a silent mutation introduced to facilitate mouse genotyping (Figure 1F). The quantification of p53 mRNA levels from WT and p53$^{Y217C/Y217C}$ MEFs next revealed similar transcription from both alleles (Figure 1G).

Deficient p53-dependent stress responses in p53$^{Y217C/Y217C}$ cells

We used western blots to analyze protein extracts from p53$^{+/+}$, p53$^{+/-}$, p53$^{+/Y217C}$, p53$^{Y217C/Y217C}$ and p53$^{-/-}$ MEFs, unstressed or treated with Nutlin, an antagonist of Mdm2, the E3 ubiquitin ligase for p53 (Vassilev et al., 2004). Results indicated a high increase in p53 abundance in untreated and Nutlin-treated p53$^{Y217C/Y217C}$ MEFs and a moderate increase in untreated and Nutlin-treated p53$^{+/Y217C}$ MEFs, compared to WT cells (Figures 2A and S2). Protein levels for p21 and Mdm2, the products of two classical p53 target genes, appeared similar in p53$^{+/+}$ and p53$^{+/Y217C}$ MEFs, and were undetectable or markedly decreased in p53$^{Y217C/Y217C}$ and p53$^{-/-}$ MEFs (Figures 2A and S2). Accordingly, p53^{Y217C} appeared unable to transactivate the *Cdkn1a/p21* and *Mdm2* genes or to bind their promoters (Figure 2B). The fractionation of cells before or after treatment with doxorubicin, a clastogenic drug, indicated that p53^{WT} accumulated in the nucleoplasm and chromatin fractions in response to DNA damage, whereas p53^{Y217C}

appeared mostly cytoplasmic in both untreated and doxorubicin-treated cells, and undetectable or barely detectable in chromatin fractions (Figures 2C and S3). Furthermore, when Nutlin-treated MEFs were analyzed by immunofluorescence, $p53^{WT}$ was only detected in nuclei, whereas $p53^{Y217C}$ could be observed in nuclear and cytoplasmic compartments (Figure 2D). We next analyzed two well-known p53-mediated responses to DNA damage, i.e. cell cycle arrest in MEFs and apoptosis in thymocytes (Kastan et al., 1992; Lowe et al., 1993). WT MEFs exposed to increasing doses of ɣ-irradiation (3 Gy or 12 Gy) exhibited significant increases in G1/S ratios, whereas G1/S ratios were similar before or after irradiation in $p53^{Y217C/Y217C}$ and $p53^{-/-}$ MEFs (Figures 2E and S4). Furthermore, thymocytes recovered from irradiated WT mice underwent a massive apoptotic response, with an almost three-fold increase in apoptotic cells after a 10 Gy irradiation. By contrast, no increase in apoptotic cells was observed upon irradiation in the thymi from $p53^{Y217C/Y217C}$ mice, and apoptotic thymocytes were equally rare in irradiated $p53^{Y217C/Y217C}$ and $p53^{-/-}$ mice (Figures 2F and S5). Together, these results indicated that the $p53^{Y217C}$ mutation altered the abundance and intracellular distribution of the p53 protein, associated with a decrease in DNA-bound protein, and that $p53^{Y217C}$ had completely lost the ability to induce cell cycle arrest and apoptosis upon DNA damage.

Impact of $p53^{Y217C}$ on mouse development and parturition

We next determined the impact of the $p53^{Y217C}$ mutation *in vivo*, by comparing mouse cohorts generated from intercrosses of heterozygous $p53^{+/-}$ or $p53^{+/Y217C}$ mice resulting from ≥ 5 backcrosses to the C57BL6/J background. Intercrosses of $p53^{+/-}$ mice are known to yield a reduced proportion of $p53^{-/-}$ mice, that is mainly due to defects in neural tube closure causing exencephaly in a fraction of $p53^{-/-}$ female embryos (Armstrong et al., 1995; Sah et al., 1995) and, to a lesser extent, to lung dysfunction affecting a fraction of $p53^{-/-}$ neonates (Tateossian et al., 2015). At weaning (on the 21st day postpartum or P21), we observed one $p53^{-/-}$ female mouse for 3.5 $p53^{-/-}$ males from $p53^{+/-}$ intercrosses, an underrepresentation of females consistent with frequencies reported in earlier studies (Armstrong et al., 1995; Sah et al., 1995). Strikingly, the underrepresentation of female mice at weaning age was even more acute for $p53^{Y217C/Y217C}$ animals, with only one $p53^{Y217C/Y217C}$ female for 19 $p53^{Y217C/Y217C}$ males from $p53^{+/Y217C}$ intercrosses (Figure 3A). We next analyzed $p53^{Y217C/Y217C}$ embryos, generated from heterozygous intercrosses, or from heterozygous-homozygous ($p53^{+/Y217C}$ x $p53^{Y217C/Y217C}$)

crosses, at embryonic days E12.5-E16.5. An underrepresentation of $p53^{Y217C/Y217C}$ female embryos was not observed, but 11/26 (42%) female embryos exhibited developmental abnormalities, including 10 with exencephaly, whereas all the male embryos appeared normal (Figure 3B). Importantly, the frequency of $p53^{Y217C/Y217C}$ female embryos with exencephaly (38.5%) was much higher than the reported frequency (0-8%) of $p53^{-/-}$ female embryos with exencephaly of C57BL/6 x 129/Sv genetic background (Donehower et al., 1992; Sah et al., 1995), suggesting a stronger effect of the $p53^{Y217C}$ mutant on female embryonic development.

In $p53^{-/-}$ female mice, exencephaly was previously correlated with stochastic aberrant X chromosome inactivation, with a decreased expression of *Xist* and an increase in bi-allelic expression of X-linked genes including *Maob*, *Pls3* and *Usp9x* (Delbridge et al., 2019). We prepared neurospheres from $p53^{+/+}$, $p53^{-/-}$ and $p53^{Y217C/Y217C}$ female embryos and quantified mRNAs for these genes in neurospheres. Compared to neurospheres from WT animals, $p53^{Y217C/Y217C}$ and $p53^{-/-}$ neurospheres exhibited an apparent decrease in *Xist* expression and significantly higher levels of *Maob*, *Pls3* and *Usp9x* (Figure S6). Thus, as for female $p53^{-/-}$ mice, aberrant chromosome X inactivation may contribute to the underrepresentation of $p53^{Y217C/Y217C}$ female mice. Of note however, defects in chromosome X inactivation did not appear to be more pronounced in $p53^{Y217C/Y217C}$ neurospheres compared to $p53^{-/-}$ neurospheres.

To further analyze the impact of the $p53^{Y217C}$ mutation during development, we also analyzed its potential effect in embryos lacking Mdm2 or Mdm4, two major p53 regulators. The embryonic lethality resulting from Mdm2 or Mdm4 loss is rescued by a concomitant p53 deficiency (Bardot et al., 2015; Finch et al., 2002; Jones et al., 1995; Migliorini et al., 2002; Montes de Oca Luna et al., 1995; Parant et al., 2001), which provides a powerful assay for analyzing the functionality of p53 mutant alleles (Bardot et al., 2015; Iwakuma et al., 2004; Marine et al., 2006; Toledo et al., 2006). We identified $Mdm2^{-/-}$ $p53^{Y217C/Y217C}$ and $Mdm4^{-/-}$ $p53^{Y217C/Y217C}$ viable mice of both sexes, consistent with a major loss of canonical WT p53 activities in the $p53^{Y217C}$ mutant (Table S1). Of note, a deficit in homozygous $p53^{Y217C/Y217C}$ females was also observed at weaning among animals lacking Mdm2 or Mdm4. Interestingly however, the female to male ratio for $p53^{Y217C/Y217C}$ animals appeared markedly increased in genetic backgrounds with Mdm4 loss (1/6) or haploinsufficiency (4/15), but only marginally increased (if at all) in genetic backgrounds with Mdm2 loss (1/11) or haploinsufficiency (1/11).

This suggested that altering the levels of p53 regulators, particularly Mdm4, might improve the survival of $p53^{Y217C/Y217C}$ females (Table S1).

Importantly, the high frequency (42%) of abnormal $p53^{Y217C/Y217C}$ female embryos at E12.5-E16.5 could only partially account for the acute deficit in $p53^{Y217C/Y217C}$ females observed at weaning, suggesting either embryonic abnormalities undetectable macroscopically, or that an important fraction of $p53^{Y217C/Y217C}$ females died later in development or postpartum. We performed additional crosses to analyze female to male ratios at postpartum day 0 or 1 (P0-P1) and observed 20 females for 18 males for $p53^{+/+}$ animals, but only 5 females for 22 males for $p53^{Y217C/Y217C}$ animals (Figure 3C). Furthermore, only one of these $p53^{Y217C/Y217C}$ females reached weaning age, and the 4 other neonates died before P2. Altogether, these data led to conclude that the $p53^{Y217C}$ mutation caused female-specific developmental abnormalities at a higher penetrance than a null allele, leading to a perinatal (late embryonic or early postpartum) lethality for most homozygous mutant females.

Interestingly, we observed that $p53^{Y217C/Y217C}$ males were fertile, and included them in some of our crosses to generate homozygous mutants at higher frequencies (Figure 3B-C and Table S1). By contrast, we were able to mate two $p53^{Y217C/Y217C}$ adult females with a $p53^{+/Y217C}$ male, and both got pregnant but had to be sacrificed due to complications while giving birth. In both cases, extended labor (> 24 hr) was the main sign of dystocia (Table S2). These observations suggest that, even for the rare $p53^{Y217C/Y217C}$ females able to reach adulthood, the $p53^{Y217C}$ mutation caused pathological traits not observed in $p53^{-/-}$ females, because the loss of p53 was not previously reported to cause dystocia (Embree-Ku and Boekelheide, 2002; Guimond et al., 1996; Hu et al., 2007). Together, our data indicated that the $p53^{Y217C}$ mutation not only abolished canonical p53 activities, but also conferred additional effects compromising female perinatal viability or parturition.

Impact of $p53^{Y217C}$ on tumorigenesis

We next analyzed the impact of the $p53^{Y217C}$ mutation on the onset and spectrum of spontaneous tumors in mice. We first compared $p53^{+/Y217C}$, $p53^{+/-}$ and $p53^{+/+}$ mouse cohorts for 2 years. $p53^{+/Y217C}$ and $p53^{+/-}$ cohorts exhibited similar spontaneous tumor onset and spectrum, with most mice developing sarcomas during their second year of life (Figure S7). Thus, at least

for tumors arising spontaneously, the p53^{Y217C} mutant protein did not appear to exert a dominant negative effect over the wildtype p53 protein.

We next compared p53$^{Y217C/Y217C}$ and p53$^{-/-}$ mouse cohorts. Because of the difficulty to generate p53$^{Y217C/Y217C}$ females, we restricted our comparison to males, to avoid potential biases that might result from different sex ratios. All p53$^{-/-}$ mice are known to die in less than 1 year, from thymic lymphomas in most cases, or more rarely from sarcomas (Donehower et al., 1992; Jacks et al., 1994). p53$^{Y217C/Y217C}$ males died faster than their p53$^{-/-}$ counterparts: all the p53$^{Y217C/Y217C}$ males were dead by the age of 7 months, whereas more than 20% of the p53$^{-/-}$ males were still alive at that age (Figure 4A). Furthermore, most p53$^{-/-}$ and p53$^{Y217C/Y217C}$ mice died from thymic lymphomas, but histological analysis of tumor organs revealed that the lymphomas in p53$^{Y217C/Y217C}$ males were more aggressive and invasive, with sites of metastases notably including the lungs and spleen (Figure 4B-C). Thus, the p53^{Y217C} mutation not only abolished canonical tumor suppressive activities but also apparently conferred oncogenic properties to the encoded protein. Consistent with this, when we performed an RNA-seq analysis of thymi from 8 weeks-old p53$^{+/+}$, p53$^{-/-}$ and p53$^{Y217C/Y217C}$ males, 81.5 % of the 717 differentially expressed genes indicated a loss of function (LOF) in the p53^{Y217C} mutant, but genes suggesting a gain of function (GOF) or a separation of function (SOF) were also observed (Figure S8A and Table S3). Of note, among the differentially expressed genes corresponding to a LOF in the p53^{Y217C} mutant were *Bbc3/Puma*, *Cdkn1a/p21* and *Zmat3* (Figure S8B), three p53-target genes known to play a major role in p53-mediated tumor suppression (Brennan et al., 2023).

We next performed a comparative analysis focusing on p53$^{Y217C/Y217C}$ and p53$^{-/-}$ thymi, which revealed 192 differentially expressed genes (Figure 5A-B, Table S4). An analysis of these data with GOrilla, the Gene Ontology enRIchment anaLysis and visuaLizAtion tool (Eden et al., 2009), indicated that 141 of these genes were associated with at least one gene ontology (GO) term, and revealed a significant enrichment for genes associated with white blood cell chemotaxis/migration and inflammation (Figure 5C and Figure S9). Among these genes were notably *Ccl17*, *Ccl9*, *Ccr3*, *Cxcl10*, *S100a8* and *S100a9*, six genes associated each with 10-15 GO terms related to white blood cell behavior or inflammation (Table S5). We next used RT-qPCR to quantify the expression of these genes in thymi from 8 weeks-old p53$^{+/+}$, p53$^{Y217C/Y217C}$ and p53$^{-/-}$ male mice, and found their expression to be significantly increased in p53$^{Y217C/Y217C}$ thymi compared to p53$^{-/-}$, or to both p53$^{+/+}$ and p53$^{-/-}$ mice, consistent with gain or separation of

function (GOF/SOF) effects in the $p53^{Y217C}$ mutant (Figure 5D). Furthermore, when we compared the transcriptomes of $p53^{Y217C/Y217C}$ and $p53^{-/-}$ thymocytes by gene set enrichment analysis (Subramanian et al., 2005), we found 13 gene sets significantly enriched in $p53^{Y217C/Y217C}$ cells (with normalized enrichment scores > 2), among which 3 ("antimicrobial peptides", "chemokine receptors bind chemokines" and "defensins") were related to an immune response (Figures 5E and S10A), consistent with an inflammatory response associated with the $p53^{Y217C}$ mutant. Other gene sets significantly enriched in $p53^{Y217C/Y217C}$ cells notably included 5 sets ("electron transport chain", "respiratory electron transport ATP synthesis by chemiosmotic coupling and heat production by uncoupling proteins", "mitochondrial translation", "respiratory electron transport" and "oxidative phosphorylation") related to mitochondria function, and 3 sets ("deposition of new CENPA-containing nucleosomes at the centromere", "arginine methyltransferases methylate histone arginines" and "PRC2 methylates histones and DNA") related to chromatin plasticity (Figure 5E and S10B-C). These gene sets, differentially expressed between $p53^{Y217C/Y217C}$ and $p53^{-/-}$ cells, might contribute to accelerated tumorigenesis in $p53^{Y217C/Y217C}$ mice, given the reported impact of inflammation, metabolism changes and epigenetic plasticity on cancer evolution (Feinberg et al., 2006; Greten and Grivennikov, 2019; Kroemer and Pouyssegur, 2008).

Discussion

In this report, we generated a mouse model with a *Trp53*^{Y217C} allele, the murine equivalent of the human hotspot mutant *TP53*^{Y220C}. The analysis of this mouse model indicated that the p53^{Y217C} mutation leads to the loss of many canonical wildtype p53 activities, notably the capacity to transactivate target genes important for tumor suppression (e.g. *Bbc3*, *Cdkn1a* and *Zmat3*). The fact that p53^{Y217C} can rescue the embryonic lethality caused by a deficiency in Mdm2 or Mdm4 is also consistent with a major loss of canonical wildtype p53 functions in this mutant.

In addition, our analyses provide evidence that the p53^{Y217C} mutation exhibits oncogenic effects. The possibility that a mutant p53 might acquire oncogenic functions was first suggested over 30 years ago (Dittmer et al., 1993), but this notion became controversial in recent years. Indeed, studies of a few p53 mutants in human acute myeloid leukemia and a mouse model of B cell lymphoma indicated that their increased tumorigenicity would result from dominant-negative effects (DNE) rather than gain-of-function (GOF), and a recent study further suggested that the putative GOF of many p53 mutants would not be required to sustain the expansion of tumors (Aubrey et al., 2018; Boettcher et al., 2019; Wang et al., 2023). Here, however, we observed accelerated tumorigenesis in p53$^{Y217C/Y217C}$ mice, but did not observe any evidence of DNE in p53$^{+/Y217C}$ animals. Importantly, the fact that p53^{Y217C} did not exhibit a DNE over the WT protein is consistent with the report that Li-Fraumeni patients carrying an heterozygous p53^{Y220C} mutation display a similar age of cancer onset than Li-Fraumeni patients with an heterozygous non-sense p53 mutation (Xu et al., 2014). Furthermore, our evidence of an oncogenic GOF leading to aggressive metastatic tumors in p53$^{Y217C/Y217C}$ male mice is consistent with the oncogenic GOF recently attributed to the p53^{Y220C} mutant in male patients with glioblastoma (Rockwell et al., 2021), or with experiments suggesting that the expression of p53^{Y220C} in p53-null cells, or its overexpression in MCF-10A cells, may increase their capacity for migration or invasion (Pal et al., 2023; Zhou et al., 2022). Our transcriptomic analyses suggested that the p53^{Y217C} mutant might accelerate tumorigenesis by promoting inflammation, a hallmark of cancer (Hanahan, 2022) previously associated with a few other hotspot p53 mutants with oncogenic GOF (Agupitan et al., 2020; Behring et al., 2019; Ham et al., 2019; Zhao et al., 2024). Interestingly, our GSEA comparison of transcriptomes from p53$^{Y217C/Y217C}$ and p53$^{-/-}$ male

thymic cells indicated differences related to inflammation and chemokine signaling, but also to mitochondria function and chromatin plasticity, and a link between inflammation, mitochondrial copper and epigenetic plasticity was recently demonstrated (Solier et al., 2023).

A striking and unexpected effect of the p53^{Y217C} mutation was its severe impact on the perinatal viability of female mice, which led to observe only 1 p53$^{Y217C/Y217C}$ female for 19 p53$^{Y217C/Y217C}$ males at weaning from heterozygous intercrosses. The perinatal lethality of p53$^{Y217C/Y217C}$ females correlated with a high frequency (38.5%) of exencephalic females at E12.5-E16.5 embryonic ages. By comparison, the female to male ratio at weaning was 1/3.5 for p53$^{-/-}$ mice, and only 0-8% of exencephalic female p53$^{-/-}$ embryos were reported in similar genetic backgrounds (Armstrong et al., 1995; Donehower et al., 1992; Sah et al., 1995). These observations provide evidence of teratogenic effects for the p53^{Y217C} mutant protein. Three other mouse p53 models were previously found to cause exencephaly at a higher frequency than a p53 null allele : p53^{NLS1}, with 3 mutations at residues 316-318 affecting a nuclear localization signal and leading to a predominantly cytoplasmic localization of p53^{NLS1} in most cells (Regeling et al., 2011); p53^{N236S}, a mouse model of p53^{N239S}, a recurrent but uncommon mutant in human cancers (Zhao et al., 2019); and Bim$^{+/-}$ p53$^{-/-}$ mice, combining p53 loss with an haploinsufficiency in the cytoplasmic proapoptotic regulator Bim/Bcl2l11 (Delbridge et al., 2019). Interestingly, the female-specific lethality of p53^{N236S} mice was proposed to result from increased *Xist* expression, whereas a decrease in *Xist* expression was observed in Bim$^{+/-}$ p53$^{-/-}$ mice, suggesting distinct causes for neural tube defects (Delbridge et al., 2019; Zhao et al., 2019). We observed decreased *Xist* expression and an increased expression of X-linked genes in p53$^{Y217C/Y217C}$ females, which is not consistent with the mechanism proposed for exencephaly in the p53^{N236S} mouse model, but might rather reflect a loss of WT p53 function (Delbridge et al., 2019). In addition, the analysis of the p53^{NLS1} and Bim$^{+/-}$ p53$^{-/-}$ mouse models make it tempting to speculate that, in female p53$^{Y217C/Y217C}$ embryos, the abundance of p53^{Y217C} in the cytoplasm might perturb mitochondria function (Blandino et al., 2020) to further promote neural tube closure defects. Consistent with this possibility, p53 mutant proteins accumulating in the cytoplasm were reported to inhibit autophagy (Morselli et al., 2008), a key determinant for mitochondrial integrity (Rambold and Lippincott-Schwartz, 2011), and autophagy impairment may promote neural tube defects (Fimia et al., 2007; Ye et al., 2020).

A particularly intriguing question is whether common mechanisms might contribute to the teratogenic effects causing the perinatal lethality of $p53^{Y217C/Y217C}$ females and the oncogenic effects accelerating tumorigenesis in $p53^{Y217C/Y217C}$ males. Interestingly, our data indicated that inflammation might promote oncogenesis in $p53^{Y217C/Y217C}$ males, and inflammation was proposed to promote neural tube defects in a few mouse models (Lian et al., 2004; Zhao et al., 2013). Furthermore CD44, which drives inflammation and cancer progression (Solier et al., 2023), was recently identified as a key gene for the diagnosis and early detection of open neural tube defects (Karthik et al., 2022). Independently, our mating attempts with $p53^{Y217C/Y217C}$ mice indicated that $p53^{Y217C/Y217C}$ pregnant females exhibited dystocia, and parturition is considered to be a finely regulated inflammatory process (Zhang and Wei, 2021). Of note, dystocia was not observed in $p53^{-/-}$ mice, but was previously reported in pregnant females with a combined deficiency of p53 and FasL (Embree-Ku and Boekelheide, 2002). The fact that $p53^{Y217C/Y217C}$ females shared phenotypic traits with both $Bim^{+/-}$ $p53^{-/-}$ mice (neural tube defects) and $FasL^{-/-}$ $p53^{-/-}$ mice (dystocia) may seem relevant, because Bim and FasL are both regulators of apoptosis and autophagy that also regulate immune responses (Sionov et al., 2015; Taylor and Ng, 2018). Altogether, these data raise the possibility that inflammation may cause accelerated tumorigenesis in $p53^{Y217C/Y217C}$ male mice and might also contribute to promote neural tube defects in $p53^{Y217C/Y217C}$ female embryos or dystocia in $p53^{Y217C/Y217C}$ pregnant females.

In conclusion, we generated a mouse model expressing $p53^{Y217C}$, the murine equivalent of human $p53^{Y220C}$, and its analysis revealed that the gain-of-function (or separation-of-function) of a hotspot mutant p53 may not be limited to oncogenic effects. This is an important notion to consider given the ever-expanding functions ascribed to p53 (Hu, 2009; Rakotopare and Toledo, 2023; Voskarides and Giannopoulou, 2023; Vousden and Lane, 2007).

Materials and Methods

LSL-Y217C construct

We used mouse genomic *Trp53* DNA from previous constructs, containing a portion of intron 1 with a LoxP-Stop-LoxP (LSL) cassette (Ventura et al., 2007) in which the puromycin-resistance gene was replaced by a neomycin-resistance gene (Simeonova et al., 2013). The point mutation (A to G) encoding a Tyr to Cys substitution (TAT to TGT) at codon 217, together with a silent mutation nearby creating a Ban II restriction site, were introduced by PCR directed mutagenesis by using primers Y217C-F and Y217C-R (See Table S6 for primer sequences). The resulting $p53^{LSL\text{-}Y217C}$ targeting vector was fully sequenced before use.

Targeting in ES Cells and Genotyping

129/SvJ embryonic stem (ES) cells were electroporated with the targeting construct linearized with Not I. Two recombinant clones, identified by long-range PCR and confirmed by internal PCR and Southern Blot, were injected into C57BL/6J blastocysts to generate chimeras, and germline transmission was verified by genotyping their offspring. *In vivo* excision of the LSL cassette was performed by breeding $p53^{+/LSL\text{-}Y217C}$ male mice with females carrying the PGK-Cre transgene (Lallemand et al., 1998) and genotyping their offspring. The $p53^{Y217C}$ ($p53^{YC}$) mutation was routinely genotyped by PCR using primers c and d (Figure 1, Table S6) followed by BanII digestion. Tumorigenesis studies were performed on mouse cohorts resulting from ≥ 5 generations of backcrosses with C57BL6/J mice. All experiments were performed according to IACUC regulations as supervised by the Ethics Committee of Institut Curie.

Cells and Cell Culture Reagents

Mouse embryonic fibroblasts (MEFs) isolated from 13.5-day embryos were cultured in a 5% CO_2 and 3% O_2 incubator, in DMEM GlutaMAX (Gibco), with 15% FBS (Biowest), 100 mM 2- mercaptoethanol (Millipore), 0.01 mM Non-Essential Amino-Acids, and penicillin/streptomycin (Gibco) for ≤ 6 passages. Cells were irradiated with a Cs γ-irradiator or treated for 24 hr with 10 mM Nutlin 3a (Sigma-Aldrich) or 10 mM Doxorubicin (Sigma-Aldrich). Neurospheres were prepared by isolating neural stem/progenitor cells (NPCs) from the lateral and median ganglionic eminences of E14.5 embryos. NPCs were cultured in a 5% CO_2

incubator, in DMEM/F12 medium (with L-Glutamine, Invitrogen) supplemented with 1% B-27 (Invitrogen), 1% N2 (Invitrogen), 0.3% glucose (Invitrogen), 25 μg/ml insulin (Sigma-Aldrich), 20 ng/ml EGF (PeproTech), 10 ng/ml bFGF (PeproTech) and penicillin/streptomycin (Gibco). Neurospheres were dissociated once a week by Accutase treatment and mechanically, then seeded at 10^6 cells per 6 cm diameter dish.

Quantitative RT-PCR

Total RNA, extracted using NucleoSpin RNA II (Macherey-Nagel), was reverse transcribed using SuperScript IV (Invitrogen). Real-time quantitative PCRs were performed as previously described (Simeonova et al., 2012), on an ABI PRISM 7500 using Power SYBR Green (Applied Biosystems). Primer sequences are reported in Table S6.

Western Blots

Cells were lysed in RIPA buffer (50 mM Tris-HCl pH 8, 150 mM NaCl, 5 mM EDTA, 0.5% deoxycholic acid, 0.1% SDS, 1% NP-40) supplemented with a Protease inhibitors cocktail (Roche) and 1 mM PMSF (Sigma). Whole-cell extracts were sonicated three times for 10 s and centrifuged at 13 000 rpm for 30 min to remove cell debris. Protein lysate concentration was determined by BCA assay (Thermo Scientific) and 30 μg of each lysate was fractionated by SDS–PAGE on a 4-12% polyacrylamide gel and transferred onto PDVF membranes (Amersham). Membranes were incubated with antibodies raised against Mdm2 (MDM2-4B2, Abcam, 1/500), p53 (CM-5, Novocastra, 1/2000), p21 (F5, Santa Cruz Biotechnology, 1/200) and actin (actin-HRP sc47778, Santa Cruz Biotechnology, 1/5000). Chemiluminescence revelation of western blots was achieved with the SuperSignal West Dura (Perbio).

ChIP Assay

ChIP analysis was performed as previously described (Simeonova et al., 2013). p53-DNA complexes were immunoprecipitated from total extracts by using 50 μg of a polyclonal antibody against p53 (FL-393, Santa Cruz Biotechnology) and 300 μg of sonicated chromatin. Rabbit IgG (Abcam) was used for control precipitation. Quantitative PCR was performed on ABI PRISM 7500. Primer sequences are reported in Table S6.

Cell Fractionation Assay

Cells were lysed in hypotonic lysis buffer (10 mM Tris pH 7.5, 10 mM NaCl, 3 mM Mgcl2, 0.3% NP-40, 10% glycerol) on ice for 10 min, then centrifuged at 4°C for 3 min at 1000g. The supernatant was recovered as the cytoplasmic fraction, and the pellet was incubated in a modified Wuarin-Schibler buffer (10 mM Tris-HCl pH 7.0, 4 mM EDTA, 0.3 M NaCl, 1 M urea, 1% NP-40) on ice for 5 min, vortexed, incubated on ice for 10 min, then centrifuged at 4°C for 3 min at 1000g. The supernatant was recovered as the nucleoplasmic fraction, and the pellet was washed, then incubated in a nuclear lysis buffer (20 mM Tris pH 7.5, 150 mM KCl, 3 mM MgCl2, 0.3% NP-40, 10% glycerol) on ice for 5 min, sonicated, then centrifuged at 13000 rpm at 4°C and the supernatant was recovered as the chromatin fraction. All buffers were supplemented with a Protease inhibitors cocktail (Roche). Cellular fractions were analyzed by western blots with antibodies against p53 (AF-1355, R&D systems, 1/600), Tubulin (ab15568, Abcam, 1/1000), Nup98 (ab50610, Abcam, 1/1000) and histone H3 (ab1791, Abcam, 1/1000). Chemiluminescence revelation was achieved with the SuperSignal West Pico or Femto (Thermoscientific) and analyzed with a ChemiDoc imaging system (Bio-Rad).

Immunofluorescence

MEFs were cultured on collagen-coated coverslips, treated with 10 μM Nutlin 3a (Sigma-Aldrich) for 24 hr and analyzed. Coverslips were stained with rabbit anti-p53 FL-393 (Santa Cruz Biotechnology), mouse anti-actin primary antibody and with Alexa Fluor 647 anti-Rabbit and Alexa Fluor 488 anti-Mouse secondary antibodies (Molecular Probes). DNA was counterstained with DAPI. Images were captured on an epifluorescence microscope using equal exposure times for all images for each fluor.

Cell-Cycle Assay

Log phase cells were irradiated at room temperature (RT) with a Cs γ-irradiator at doses of 3 or 12 Gy, incubated for 24 hr, then pulse labeled for 1 hr with BrdU (10 μM), fixed in 70% ethanol, double stained with FITC anti-BrdU and propidium iodide, and analyzed by flow cytometry with a BD Biosciences FACSort and the FlowJo software.

Apoptosis Assay

Six to eight weeks-old mice were left untreated or submitted to 10 Gy whole-body ɣ-irradiation. Mice were sacrificed 4 hr later and thymi were extracted. Thymocytes were recovered by filtration through a 70 µm smash, stained with Annexin V-FITC Apoptosis detection kit (Abcam) and propidium iodide, then analyzed with a LSRII FACS machine. Data were analyzed using Flowjo software.

Histology

Organs were fixed in formol 4% for 24 hr, then ethanol 70%, and embedded in paraffin wax. Serial sections were stained as described (Simeonova et al., 2013), with hematoxylin and eosin using standard procedures.

RNA-Seq analysis

Total RNA was extracted from the thymi of 8 weeks-old asymptomatic male mice using nucleospin RNA II (Macherey-Nagel). The quality of RNA was checked with Bioanalyzer Agilent 2100 and RNAs with a RIN (RNA integrity number) $\geq$ 7 were retained for further analysis. RNA was depleted from ribosomal RNA, then converted into cDNA libraries using a TruSeq Stranded Total Library preparation kit (Illumina). Paired-end sequencing was performed on an Illumina MiSeq platform. Reads were mapped to the mouse genome version GRCm38 and counted on gene annotation gencode.vM18 with featureCounts (Liao et al., 2014). Differentially expressed genes with an adjusted p-value < 0.05 were identified using the DESeq2 R package (Love et al., 2014).

Gene Ontology analysis

Gene ontology analysis of differentially expressed genes was performed by using the GOrilla (Technion) software as previously described (Rakotopare et al., 2023). Enrichment analyses were carried out by comparing the list of 192 differentially expressed genes between $p53^{Y217C/Y217C}$ and $p53^{-/-}$ thymi to the full list of genes (background), with ontology searches for biological processes and default *P*-value settings (10^{-3}).

Gene set enrichment analysis

Gene set enrichment analysis was performed by using the GSEA software with canonical pathway gene sets from the Mouse Molecular Signature Database (MSigDB) (Subramanian et al., 2005). Gene sets that displayed a normalized enrichment score (NES) > 2, a nominal (NOM) P-value <0.01, and a false discovery rate (FDR) q-value < 0.01 were regarded as significantly enriched.

Statistical analyses

The Student's *t* test was used in all figures to analyze differences between two groups of values. For the proportions of mice at weaning, the observed mice count was compared to the expected count according to Mendel's distribution and a Chi-square (χ^2) test, and a Fischer's test was applied to compare frequencies of mutant females. Survival curves were analyzed with log-rank Mantel-Cox tests. Analyses were performed by using GraphPad Prism, and values of $P \leq 0.05$ were considered significant.

Data availability

RNA sequencing data have been deposited in the Gene Expression Omnibus (GEO) under the accession code GSE248936.

Acknowledgments

This project was supported by grants attributed to F.T., from the Ligue Nationale Contre le Cancer, the Fondation ARC pour la recherche sur le Cancer and the Gefluc. S.J., E.E. and J.R. were PhD fellows of the Ministère de la Recherche, and S.J. and E.E. received additional support from the Fondation ARC; M.G. was paid by European Research Council 875532-Prostator-ERC-2019-PoC attributed to A.M. We thank V. Volochtchouk and M. Licaj for technical help, A. Fajac for comments on the manuscript, and the following members of the Institut Curie platforms: I. Grandjean, H. Gautier, C. Daviaud, M. Garcia, M. Verlhac, A. Fosse and D. Andreau (animal facility); S. Baulande and S. Lameiras (NGS); M. Huerre, A. Nicolas and R. Leclere (histopathology); Z. Maciorowski, A. Viguier and S. Grondin (flow cytometry).

Author Contributions

Conceptualization: F.T.; investigation: S.J., E.E., J.R., V.L., I.S, B.B., F.T.; formal analysis: M.G., B.B., F.T., A.M.; supervision, writing and visualization: F.T., B.B; project administration and funding acquisition: F.T.

Declaration of interests

The authors declare no competing financial interests.

References

Agupitan AD, Neeson P, Williams S, Howitt J, Haupt S, Haupt Y. 2020. P53: A guardian of immunity becomes its saboteur through mutation. *Int J Mol Sci* **21**:3452. doi:10.3390/ijms21103452

Amelio I, Melino G. 2020. Context is everything: extrinsic signalling and gain-of-function p53 mutants. *Cell Death Discov* **6**:16. doi:10.1038/s41420-020-0251-x

Armstrong JF, Kaufman MH, Harrison DJ, Clarke AR. 1995. High-frequency developmental abnormalities in p53-deficient mice. *Curr Biol* **5**:931–936. doi:10.1016/s0960-9822(95)00183-7

Aubrey BJ, Janic A, Chen Y, Chang C, Lieschke EC, Diepstraten ST, Kueh AJ, Bernardini JP, Dewson G, O'Reilly LA, Whitehead L, Voss AK, Smyth GK, Strasser A, Kelly GL. 2018. Mutant TRP53 exerts a target gene-selective dominant-negative effect to drive tumor development. *Genes Dev* **32**:1420–1429. doi:10.1101/gad.314286.118

Bardot B, Bouarich-Bourimi R, Leemput J, Lejour V, Hamon A, Plancke L, Jochemsen AG, Simeonova I, Fang M, Toledo F. 2015. Mice engineered for an obligatory Mdm4 exon skipping express higher levels of the Mdm4-S isoform but exhibit increased p53 activity. *Oncogene* **34**:2943–2948. doi:10.1038/onc.2014.230

Beckerman R, Prives C. 2010. Transcriptional regulation by p53. *Cold Spring Harb Perspect Biol* **2**:a000935. doi:10.1101/cshperspect.a000935

Behring M, Vazquez AI, Cui X, Irvin MR, Ojesina AI, Agarwal S, Manne U, Shrestha S. 2019. Gain of function in somatic *TP53* mutations is associated with immune-rich breast tumors and changes in tumor-associated macrophages. *Molec Genet Genomic Med* **7**:e1001. doi:10.1002/mgg3.1001

Blandino G, Valenti F, Sacconi A, Di Agostino S. 2020. Wild type- and mutant p53 proteins in mitochondrial dysfunction: emerging insights in cancer disease. *Semin Cell Dev Biol* **98**:105–117. doi:10.1016/j.semcdb.2019.05.011

Boettcher S, Miller PG, Sharma R, McConkey M, Leventhal M, Krivtsov AV, Giacomelli AO, Wong W, Kim J, Chao S, Kurppa KJ, Yang X, Milenkowic K, Piccioni F, Root DE, Rücker FG, Flamand Y, Neuberg D, Lindsley RC, Jänne PA, Hahn WC, Jacks T, Döhner H, Armstrong SA, Ebert BL. 2019. A dominant-negative effect drives selection of TP53 missense mutations in myeloid malignancies. *Science* **365**:599–604. doi:10.1126/science.aax3649

Bouaoun L, Sonkin D, Ardin M, Hollstein M, Byrnes G, Zavadil J, Olivier M. 2016. TP53 variations in human cancers: new lessons from the IARC TP53 database and genomics data. *Hum Mutat* **37**:865–876. doi:10.1002/humu.23035

Brennan MS, Brinkmann K, Romero Sola G, Healey G, Gibson L, Gangoda L, Potts MA, Lieschke E, Wilcox S, Strasser A, Herold MJ, Janic A. 2023. Combined absence of TRP53 target genes ZMAT3, PUMA and p21 cause a high incidence of cancer in mice. *Cell Death Differ*. doi:10.1038/s41418-023-01250-w

Delbridge ARD, Kueh AJ, Ke F, Zamudio NM, El-Saafin F, Jansz N, Wang G-Y, Iminitoff M, Beck T, Haupt S, Hu Y, May RE, Whitehead L, Tai L, Chiang W, Herold MJ, Haupt Y, Smyth GK, Thomas T, Blewitt ME, Strasser A, Voss AK. 2019. Loss of p53 causes stochastic aberrant X-chromosome inactivation and female-specific neural tube defects. *Cell Rep* **27**:442-454.e5. doi:10.1016/j.celrep.2019.03.048

Dibra D, Xiong S, Moyer SM, El-Naggar AK, Qi Y, Su X, Kong EK, Korkut A, Lozano G. 2024. Mutant p53 protects triple-negative breast adenocarcinomas from ferroptosis in vivo.

Sci Adv **10**:eadk1835. doi:10.1126/sciadv.adk1835
Dittmer D, Pati S, Zambetti G, Chu S, Teresky AK, Moore M, Finlay C, Levine AJ. 1993. Gain of function mutations in p53. *Nat Genet* **4**:42–46. doi:10.1038/ng0593-42
Donehower LA, Harvey M, Slagle BL, McArthur MJ, Montgomery CA, Butel JS, Bradley A. 1992. Mice deficient for p53 are developmentally normal but susceptible to spontaneous tumours. *Nature* **356**:215–221. doi:10.1038/356215a0
Dumbrava E, Johnson M, Tolcher A, Shapiro G, Thompson J, El-Khoueiry A, Vandross A, Kummar S, Parikh A, Munster P, Daly E, De Leon L, Khaddar M, LeDuke K, Robell K, Sheehan L, St. Louis M, Wiebesiek A, Alland L, Schram A. 2022. First-in-human study of PC14586, a small molecule structural corrector of Y220C mutant p53, in patients with advanced solid tumors harboring a TP53 Y220C mutation. *J Clin Oncol* **40**:suppl 3003. doi:10.1200/JCO.2022.40.16_suppl.3003
Eden E, Navon R, Steinfeld I, Lipson D, Yakhini Z. 2009. GOrilla: a tool for discovery and visualization of enriched GO terms in ranked gene lists. *BMC Bioinformatics* **10**:48. doi:10.1186/1471-2105-10-48
Embree-Ku M, Boekelheide K. 2002. Absence of p53 and FasL has sexually dimorphic effects on both development and reproduction. *Exp Biol Med* **227**:545–553. doi:10.1177/153537020222700720
Feinberg AP, Ohlsson R, Henikoff S. 2006. The epigenetic progenitor origin of human cancer. *Nat Rev Genet* **7**:21–33. doi:10.1038/nrg1748
Fimia GM, Stoykova A, Romagnoli A, Giunta L, Di Bartolomeo S, Nardacci R, Corazzari M, Fuoco C, Ucar A, Schwartz P, Gruss P, Piacentini M, Chowdhury K, Cecconi F. 2007. Ambra1 regulates autophagy and development of the nervous system. *Nature* **447**:1121–1125. doi:10.1038/nature05925
Finch RA, Donoviel DB, Potter D, Shi M, Fan A, Freed DD, Wang C-Y, Zambrowicz BP, Ramirez-Solis R, Sands AT, Zhang N. 2002. Mdmx is a negative regulator of p53 activity in vivo. *Cancer Res* **62**:3221–3225.
Gencel-Augusto J, Lozano G. 2020. p53 tetramerization: at the center of the dominant-negative effect of mutant p53. *Genes Dev* **34**:1128–1146. doi:10.1101/gad.340976.120
Greten FR, Grivennikov SI. 2019. Inflammation and cancer: triggers, mechanisms, and consequences. *Immunity* **51**:27–41. doi:10.1016/j.immuni.2019.06.025
Guimond MJ, Wang B, Fujita J, Terhorst C, Croy BA. 1996. Pregnancy-associated uterine granulated metrial gland cells in mutant and transgenic mice. *Am J Reprod Immunol* **35**:501–509. doi:10.1111/j.1600-0897.1996.tb00049.x
Hainaut P, Pfeifer GP. 2016. Somatic TP53 mutations in the era of genome sequencing. *Cold Spring Harb Perspect Med* **6**:a026179. doi:10.1101/cshperspect.a026179
Ham SW, Jeon H-Y, Jin X, Kim E-J, Kim J-K, Shin YJ, Lee Y, Kim SH, Lee SY, Seo S, Park MG, Kim H-M, Nam D-H, Kim H. 2019. TP53 gain-of-function mutation promotes inflammation in glioblastoma. *Cell Death Differ* **26**:409–425. doi:10.1038/s41418-018-0126-3
Hanahan D. 2022. Hallmarks of cancer: new dimensions. *Cancer Discovery* **12**:31–46. doi:10.1158/2159-8290.CD-21-1059
Hanel W, Marchenko N, Xu S, Yu SX, Weng W, Moll U. 2013. Two hot spot mutant p53 mouse models display differential gain of function in tumorigenesis. *Cell Death Differ* **20**:898–909. doi:10.1038/cdd.2013.17
Hollstein M, Sidransky D, Vogelstein B, Harris CC. 1991. p53 mutations in human cancers.

Science **253**:49–53. doi:10.1126/science.1905840
Hu W. 2009. The role of p53 gene family in reproduction. *Cold Spring Harb Perspect Biol* **1**:a001073. doi:10.1101/cshperspect.a001073
Hu W, Feng Z, Teresky AK, Levine AJ. 2007. p53 regulates maternal reproduction through LIF. *Nature* **450**:721–724. doi:10.1038/nature05993
Humpton TJ, Hock AK, Maddocks ODK, Vousden KH. 2018. p53-mediated adaptation to serine starvation is retained by a common tumour-derived mutant. *Cancer Metab* **6**:18. doi:10.1186/s40170-018-0191-6
Iwakuma T, Parant JM, Fasulo M, Zwart E, Jacks T, de Vries A, Lozano G. 2004. Mutation at p53 serine 389 does not rescue the embryonic lethality in mdm2 or mdm4 null mice. *Oncogene* **23**:7644–7650. doi:10.1038/sj.onc.1207793
Jacks T, Remington L, Williams BO, Schmitt EM, Halachmi S, Bronson RT, Weinberg RA. 1994. Tumor spectrum analysis in p53-mutant mice. *Curr Biol* **4**:1–7. doi:10.1016/s0960-9822(00)00002-6
Joerger AC, Ang HC, Fersht AR. 2006. Structural basis for understanding oncogenic p53 mutations and designing rescue drugs. *Proc Natl Acad Sci U S A* **103**:15056–15061. doi:10.1073/pnas.0607286103
Jones SN, Roe AE, Donehower LA, Bradley A. 1995. Rescue of embryonic lethality in Mdm2-deficient mice by absence of p53. *Nature* **378**:206–208. doi:10.1038/378206a0
Kadosh E, Snir-Alkalay I, Venkatachalam A, May S, Lasry A, Elyada E, Zinger A, Shaham M, Vaalani G, Mernberger M, Stiewe T, Pikarsky E, Oren M, Ben-Neriah Y. 2020. The gut microbiome switches mutant p53 from tumour-suppressive to oncogenic. *Nature* **586**:133–138. doi:10.1038/s41586-020-2541-0
Karthik KV, Rajalingam A, Shivashankar M, Ganjiwale A. 2022. Recursive feature elimination-based biomarker identification for open neural tube defects. *Curr Genomics* **23**:195–206. doi:10.2174/1389202923666220511162038
Kastan MB, Zhan Q, el-Deiry WS, Carrier F, Jacks T, Walsh WV, Plunkett BS, Vogelstein B, Fornace AJ. 1992. A mammalian cell cycle checkpoint pathway utilizing p53 and GADD45 is defective in ataxia-telangiectasia. *Cell* **71**:587–597. doi:10.1016/0092-8674(92)90593-2
Kennedy MC, Lowe SW. 2022. Mutant p53: it's not all one and the same. *Cell Death Differ* **29**:983–987. doi:10.1038/s41418-022-00989-y
Kim E, Deppert W. 2007. Interactions of mutant p53 with DNA: guilt by association. *Oncogene* **26**:2185–2190. doi:10.1038/sj.onc.1210312
Kim MP, Lozano G. 2018. Mutant p53 partners in crime. *Cell Death Differ* **25**:161–168. doi:10.1038/cdd.2017.185
Kotler E, Shani O, Goldfeld G, Lotan-Pompan M, Tarcic O, Gershoni A, Hopf TA, Marks DS, Oren M, Segal E. 2018. A systematic p53 mutation library links differential functional impact to cancer mutation pattern and evolutionary conservation. *Mol Cell* **71**:178-190.e8. doi:10.1016/j.molcel.2018.06.012
Kroemer G, Pouyssegur J. 2008. Tumor cell metabolism: cancer's Achilles' heel. *Cancer Cell* **13**:472–482. doi:10.1016/j.ccr.2008.05.005
Lallemand Y, Luria V, Haffner-Krausz R, Lonai P. 1998. Maternally expressed PGK-Cre transgene as a tool for early and uniform activation of the Cre site-specific recombinase. *Transgenic Res* **7**:105–112. doi:10.1023/a:1008868325009
Lian Q, Dheen ST, Liao D, Tay SSW. 2004. Enhanced inflammatory response in neural tubes of embryos derived from diabetic mice exposed to a teratogen. *J of Neuroscience Research*

75:554–564. doi:10.1002/jnr.20006
Liao Y, Smyth GK, Shi W. 2014. featureCounts: an efficient general purpose program for assigning sequence reads to genomic features. *Bioinformatics* **30**:923–930. doi:10.1093/bioinformatics/btt656
Love MI, Huber W, Anders S. 2014. Moderated estimation of fold change and dispersion for RNA-seq data with DESeq2. *Genome Biol* **15**:550. doi:10.1186/s13059-014-0550-8
Lowe SW, Schmitt EM, Smith SW, Osborne BA, Jacks T. 1993. p53 is required for radiation-induced apoptosis in mouse thymocytes. *Nature* **362**:847–849. doi:10.1038/362847a0
Marine J-C, Francoz S, Maetens M, Wahl G, Toledo F, Lozano G. 2006. Keeping p53 in check: essential and synergistic functions of Mdm2 and Mdm4. *Cell Death Differ* **13**:927–934. doi:10.1038/sj.cdd.4401912
McCann JJ, Vasilevskaya IA, McNair C, Gallagher P, Neupane NP, De Leeuw R, Shafi AA, Dylgjeri E, Mandigo AC, Schiewer MJ, Knudsen KE. 2022. Mutant p53 elicits context-dependent pro-tumorigenic phenotypes. *Oncogene* **41**:444–458. doi:10.1038/s41388-021-01903-5
Migliorini D, Lazzerini Denchi E, Danovi D, Jochemsen A, Capillo M, Gobbi A, Helin K, Pelicci PG, Marine J-C. 2002. Mdm4 (Mdmx) regulates p53-induced growth arrest and neuronal cell death during early embryonic mouse development. *Mol Cell Biol* **22**:5527–5538. doi:10.1128/MCB.22.15.5527-5538.2002
Montes de Oca Luna R, Wagner DS, Lozano G. 1995. Rescue of early embryonic lethality in Mdm2-deficient mice by deletion of p53. *Nature* **378**:203–206. doi:10.1038/378203a0
Morselli E, Tasdemir E, Maiuri MC, Galluzzi L, Kepp O, Criollo A, Vicencio JM, Soussi T, Kroemer G. 2008. Mutant p53 protein localized in the cytoplasm inhibits autophagy. *Cell Cycle* **7**:3056–3061. doi:10.4161/cc.7.19.6751
Pal A, Gonzalez-Malerva L, Eaton S, Xu C, Zhang Y, Grief D, Sakala L, Nwekwo L, Zeng J, Christensen G, Gupta C, Streitwieser E, Singharoy A, Park JG, LaBaer J. 2023. Multidimensional quantitative phenotypic and molecular analysis reveals neomorphic behaviors of p53 missense mutants. *NPJ Breast Cancer* **9**:78. doi:10.1038/s41523-023-00582-7
Parant J, Chavez-Reyes A, Little NA, Yan W, Reinke V, Jochemsen AG, Lozano G. 2001. Rescue of embryonic lethality in Mdm4-null mice by loss of Trp53 suggests a nonoverlapping pathway with MDM2 to regulate p53. *Nat Genet* **29**:92–95. doi:10.1038/ng714
Pfister NT, Prives C. 2017. Transcriptional regulation by wild-type and cancer-related mutant forms of p53. *Cold Spring Harb Perspect Med* **7**:a026054. doi:10.1101/cshperspect.a026054
Rakotopare J, Lejour V, Duval C, Eldawra E, Escoffier H, Toledo F. 2023. A systematic approach identifies p53-DREAM pathway target genes associated with blood or brain abnormalities. *Dis Model Mech* **16**:dmm050376. doi:10.1242/dmm.050376
Rakotopare J, Toledo F. 2023. p53 in the molecular circuitry of bone marrow failure syndromes. *Int J Mol Sci* **24**:14940. doi:10.3390/ijms241914940
Rambold AS, Lippincott-Schwartz J. 2011. Mechanisms of mitochondria and autophagy crosstalk. *Cell Cycle* **10**:4032–4038. doi:10.4161/cc.10.23.18384
Regeling A, Armata HL, Gallant J, Jones SN, Sluss HK. 2011. Mice defective in p53 nuclear localization signal 1 exhibit exencephaly. *Transgenic Res* **20**:899–912. doi:10.1007/s11248-010-9468-4
Rockwell NC, Yang W, Warrington NM, Staller MV, Griffith M, Griffith OL, Gurnett CA, Cohen BA, Baldridge D, Rubin JB. 2021. Sex- and mutation-specific p53 gain-of-function

activity in gliomagenesis. *Cancer Research Communications* **1**:148–163. doi:10.1158/2767-9764.CRC-21-0026

Sah VP, Attardi LD, Mulligan GJ, Williams BO, Bronson RT, Jacks T. 1995. A subset of p53-deficient embryos exhibit exencephaly. *Nat Genet* **10**:175–180. doi:10.1038/ng0695-175

Shirole N, Pal D, Kastenhuber E, Senturk S, Boroda J, Pisterzi P, Miller M, Munoz G, Anderluh M, Ladanyi M, Lowe S, Sordella R. 2016. TP53 exon-6 truncating mutations produce separation of function isoforms with pro-tumorigenic functions. *Elife* e17929. doi:doi: 10.7554/eLife.17929

Simeonova I, Jaber S, Draskovic I, Bardot B, Fang M, Bouarich-Bourimi R, Lejour V, Charbonnier L, Soudais C, Bourdon J-C, Huerre M, Londono-Vallejo A, Toledo F. 2013. Mutant mice lacking the p53 C-terminal domain model telomere syndromes. *Cell Rep* **3**:2046–2058. doi:10.1016/j.celrep.2013.05.028

Simeonova I, Lejour V, Bardot B, Bouarich-Bourimi R, Morin A, Fang M, Charbonnier L, Toledo F. 2012. Fuzzy tandem repeats containing p53 response elements may define species-specific p53 target genes. *PLoS Genet* **8**:e1002731. doi:10.1371/journal.pgen.1002731

Sionov RV, Vlahopoulos SA, Granot Z. 2015. Regulation of Bim in health and disease. *Oncotarget* **6**:23058–23134. doi:10.18632/oncotarget.5492

Solier S, Müller S, Cañeque T, Versini A, Mansart A, Sindikubwabo F, Baron L, Emam L, Gestraud P, Pantoș GD, Gandon V, Gaillet C, Wu T-D, Dingli F, Loew D, Baulande S, Durand S, Sencio V, Robil C, Trottein F, Péricat D, Näser E, Cougoule C, Meunier E, Bègue A-L, Salmon H, Manel N, Puisieux A, Watson S, Dawson MA, Servant N, Kroemer G, Annane D, Rodriguez R. 2023. A druggable copper-signalling pathway that drives inflammation. *Nature* **617**:386–394. doi:10.1038/s41586-023-06017-4

Stein Y, Aloni-Grinstein R, Rotter V. 2020. Mutant p53 oncogenicity: dominant-negative or gain-of-function? *Carcinogenesis* **41**:1635–1647. doi:10.1093/carcin/bgaa117

Subramanian A, Tamayo P, Mootha VK, Mukherjee S, Ebert BL, Gillette MA, Paulovich A, Pomeroy SL, Golub TR, Lander ES, Mesirov JP. 2005. Gene set enrichment analysis: a knowledge-based approach for interpreting genome-wide expression profiles. *Proc Natl Acad Sci USA* **102**:15545–15550. doi:10.1073/pnas.0506580102

Tateossian H, Morse S, Simon MM, Dean CH, Brown SDM. 2015. Interactions between the otitis media gene, *Fbxo11* , and *p53* in the mouse embryonic lung. *Disease Models & Mechanisms* dmm.022426. doi:10.1242/dmm.022426

Taylor AW, Ng TF. 2018. Negative regulators that mediate ocular immune privilege. *J Leukoc Biol*. doi:10.1002/JLB.3MIR0817-337R

Toledo F, Krummel KA, Lee CJ, Liu C-W, Rodewald L-W, Tang M, Wahl GM. 2006. A mouse p53 mutant lacking the proline-rich domain rescues Mdm4 deficiency and provides insight into the Mdm2-Mdm4-p53 regulatory network. *Cancer Cell* **9**:273–285. doi:10.1016/j.ccr.2006.03.014

Tseng T-H, Wang C-J, Lee Y-J, Shao Y-C, Shen C-H, Lee K-C, Tung S-Y, Kuo H-C. 2022. Suppression of the proliferation of Huh7 hepatoma cells involving the downregulation of mutant p53 protein and inactivation of the STAT 3 pathway with ailanthoidol. *Int J Mol Sci* **23**:5102. doi:10.3390/ijms23095102

Vassilev LT, Vu BT, Graves B, Carvajal D, Podlaski F, Filipovic Z, Kong N, Kammlott U, Lukacs C, Klein C, Fotouhi N, Liu EA. 2004. In vivo activation of the p53 pathway by small-molecule antagonists of MDM2. *Science* **303**:844–848. doi:10.1126/science.1092472

Ventura A, Kirsch DG, McLaughlin ME, Tuveson DA, Grimm J, Lintault L, Newman J, Reczek

EE, Weissleder R, Jacks T. 2007. Restoration of p53 function leads to tumour regression in vivo. *Nature* **445**:661–665. doi:10.1038/nature05541

Vikhanskaya F, Lee MK, Mazzoletti M, Broggini M, Sabapathy K. 2007. Cancer-derived p53 mutants suppress p53-target gene expression--potential mechanism for gain of function of mutant p53. *Nucleic Acids Res* **35**:2093–2104. doi:10.1093/nar/gkm099

Voskarides K, Giannopoulou N. 2023. The role of TP53 in adaptation and evolution. *Cells* **12**:512. doi:10.3390/cells12030512

Vousden KH, Lane DP. 2007. p53 in health and disease. *Nat Rev Mol Cell Biol* **8**:275–283. doi:10.1038/nrm2147

Wang Z, Burigotto M, Ghetti S, Vaillant F, Tan T, Capaldo B, Palmieri M, Hirokawa Y, Tai L, Simpson D, Chang C, Huang A, Lieschke E, Diepstraten S, Kaloni D, Riffkin C, Huang D, Li Wai Suen C, Garnham A, Gibbs P, Visvader J, Sieber O, Herold M, Fava L, Kelly G, Strasser A. 2023. Loss-of-function but not gain-of-function properties of mutant TP53 are critical for the proliferation, survival and metastasis of a broad range of cancer cells. *Cancer Discov*. doi:10.1158/2159-8290.CD-23-0402.

Xiong S, Chachad D, Zhang Y, Gencel-Augusto J, Sirito M, Pant V, Yang P, Sun C, Chau G, Qi Y, Su X, Whitley EM, El-Naggar AK, Lozano G. 2022. Differential gain-of-function activity of three p53 hotspot mutants *in vivo*. *Cancer Research* **82**:1926–1936. doi:10.1158/0008-5472.CAN-21-3376

Xu J, Qian J, Hu Y, Wang J, Zhou X, Chen H, Fang J-Y. 2014. Heterogeneity of Li-Fraumeni syndrome links to unequal gain-of-function effects of p53 mutations. *Sci Rep* **4**:4223. doi:10.1038/srep04223

Ye J, Tong Y, Lv J, Peng R, Chen S, Kuang L, Su K, Zheng Y, Zhang T, Zhang F, Jin L, Yang X, Wang H. 2020. Rare mutations in the autophagy-regulating gene AMBRA1 contribute to human neural tube defects. *Hum Mutat* **41**:1383–1393. doi:10.1002/humu.24028

Zhang X, Wei H. 2021. Role of decidual natural killer cells in human pregnancy and related pregnancy complications. *Front Immunol* **12**:728291. doi:10.3389/fimmu.2021.728291

Zhao J, Tian Y, Zhang H, Qu L, Chen Y, Liu Q, Luo Y, Wu X. 2019. p53 mutant $p53^{N236S}$ induces neural tube defects in female embryos. *Int J Biol Sci* **15**:2006–2015. doi:10.7150/ijbs.31451

Zhao M, Chen Y-H, Dong X-T, Zhou J, Chen X, Wang H, Wu S-X, Xia M-Z, Zhang C, Xu D-X. 2013. Folic acid protects against lipopolysaccharide-induced preterm delivery and intrauterine growth restriction through its anti-inflammatory effect in mice. *PLoS ONE* **8**:e82713. doi:10.1371/journal.pone.0082713

Zhao M, Wang T, Gleber-Netto FO, Chen Z, McGrail DJ, Gomez JA, Ju W, Gadhikar MA, Ma W, Shen L, Wang Q, Tang X, Pathak S, Raso MG, Burks JK, Lin S-Y, Wang J, Multani AS, Pickering CR, Chen J, Myers JN, Zhou G. 2024. Mutant p53 gains oncogenic functions through a chromosomal instability-induced cytosolic DNA response. *Nat Commun* **15**:180. doi:10.1038/s41467-023-44239-2

Zhou J, Luo J, Li Peiwei, Zhou Y, Li Peichao, Wang F, Mallio CA, Rossi G, Jalal AH, Filipovic N, Tian Z, Zhao X. 2022. Triptolide promotes degradation of the unfolded gain-of-function Tp53R175H/Y220C mutant protein by initiating heat shock protein 70 transcription in non-small cell lung cancer. *Transl Lung Cancer Res* **11**:802–816. doi:10.21037/tlcr-22-312

Figures

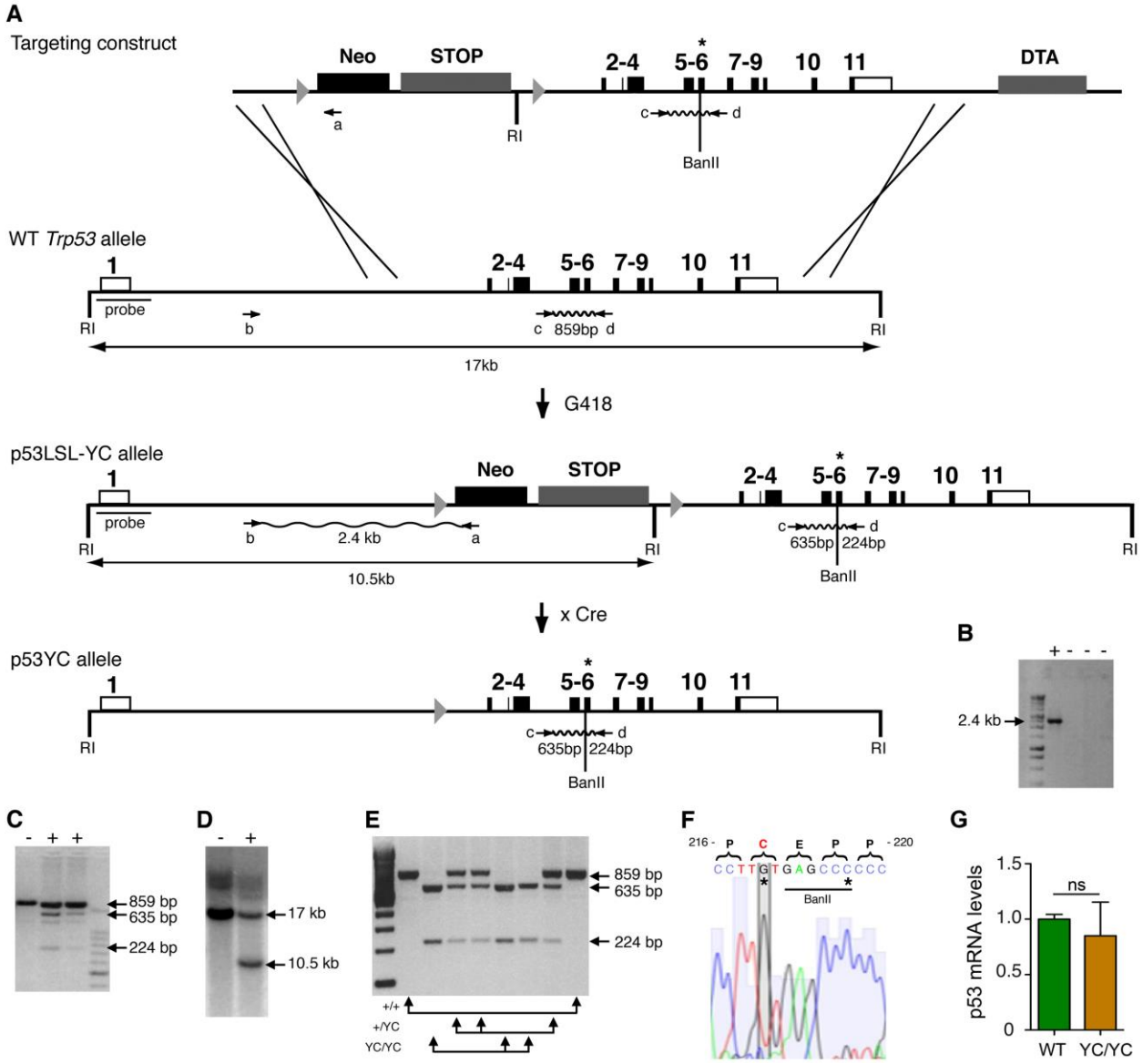

Figure 1. Targeting the Y217C missense mutation at the mouse *Trp53* locus.
(A) Targeting strategy. The *Trp53* gene is within a 17 kb-long EcoRI (RI) fragment (black boxes are for coding sequences and white boxes for UTRs). The targeting construct contains: (1) a 1.5 kb-long 5' homology region; (2) a Lox-Stop-Lox (LSL) cassette with a *neomycin* selection gene (Neo), four transcriptional stops (STOP) and an EcoRI site, flanked by LoxP sites (arrowheads); (3) p53 exons, including the Y217C (YC) missense mutation in exon 6 (asterisk) and an additional BanII site; (4) a 2.8 kb-long 3' homology region; and (5) the diphteria α-toxin (DTA) gene for targeting enrichment. Proper recombinants with a $p53^{LSL\text{-}Y217C}$ allele were identified by a 2.4 kb-long band after PCR with primers a and b, and confirmed by bands of 635 and 224 bp after PCR with primers c and d and BanII digestion. They were also verified by Southern blot with the indicated probe as containing a 10.5 kb EcoRI band. Two recombinant ES clones were

injected into blastocysts to generate chimeras, and germline transmission was verified by genotyping with primers c and d and BanII digestion. Excision of the LSL cassette was performed *in vivo*, by breeding $p53^{+/LSL\text{-}Y217C}$ male mice with females carrying the PGK-Cre transgene. **(B-D)** Screening of recombinant ES clones (+) by PCR with primers a and b (B); PCR with primers c and d then BanII digestion (C); Southern blot (D). **(E)** Genotyping of mouse embryonic fibroblasts (MEFs) from an intercross of $p53^{+/Y217C}$ mice, by PCR with primers c and d and BanII digestion. **(F)** $p53^{Y217C}$ sequence around codon 217. The introduced Y217C missense mutation and the mutation creating an additional BanII restriction site are highlighted (asterisks). **(G)** WT and $p53^{Y217C/Y217C}$ MEFs express similar p53 mRNA levels. Total RNA was extracted, then p53 mRNAs were quantified by real-time qPCR, normalized to control mRNAs and the amount in WT cells was assigned the value of 1. Primer sequences are listed in Table S6.

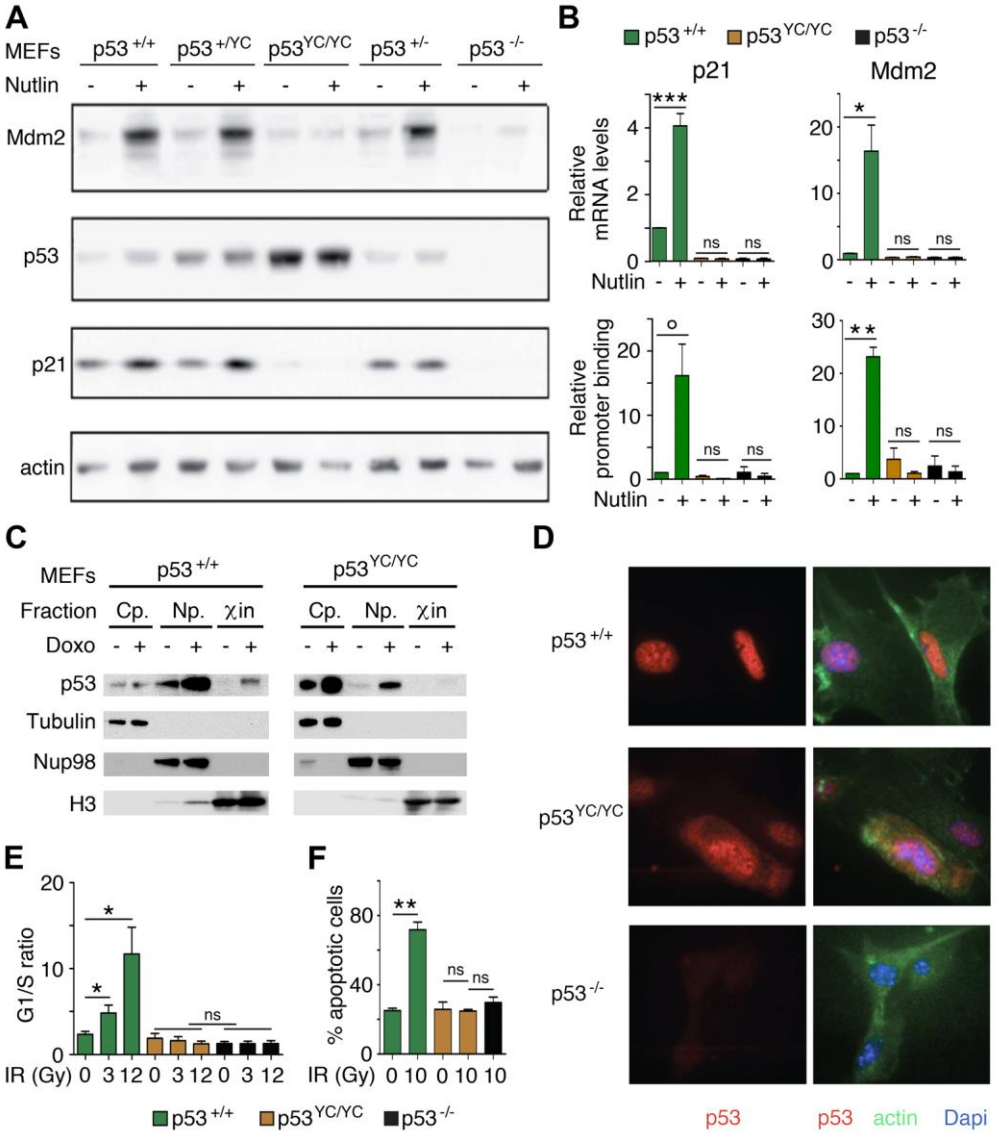

Figure 2. p53$^{Y217C/Y217C}$ cells exhibit alterations in p53 abundance and subcellular localization and defective responses to DNA damage.

(A) Increased p53 protein levels in p53$^{Y217C/Y217C}$ and p53$^{+/Y217C}$ MEFs. MEFs of the indicated genotypes were treated or not with 10 μM Nutlin 3a for 24 h, then protein extracts were immunoblotted with antibodies against Mdm2, p53, p21 and actin. **(B)** The transactivation of classical p53 target genes *Cdkn1a/p21* and *Mdm2* is impaired in p53$^{Y217C/Y217C}$ cells. WT, p53$^{Y217C/Y217C}$ and p53$^{-/-}$ MEFs were treated as in (A), then (top) mRNAs were quantified in 5-6 independent experiments using real-time PCR, with results normalized to control mRNAs and mean RNA amounts in unstressed p53$^{+/+}$ cells assigned a value of 1; or (bottom) ChIP assays were performed at the *Cdkn1a* and *Mdm2* promoters in 2-3 independent experiments with an antibody against p53 or rabbit IgG as a negative control. Immunoprecipitates were quantified using real-time PCR, normalized to data over an irrelevant region, and the amount in unstressed p53$^{+/+}$ cells was assigned a value of 1. **(C)** Assessment of p53^{WT} and p53^{Y217C} subcellular localization by cellular fractionation. WT and p53$^{Y217C/Y217C}$ MEFs were treated or not with doxorubicin for 24 hr, submitted to cellular fractionation, then protein extracts were

immunoblotted with antibodies against p53 or the fraction controls Tubulin for cytoplasm (Cp.), Nup98 for nucleoplasm (Np.) and histone H3 for chromatin (χin). **(D)** Assessment of $p53^{WT}$ and $p53^{Y217C}$ subcellular localization by immunofluorescence. WT, $p53^{Y217C/Y217C}$ and $p53^{-/-}$ MEFs were treated with 10 μM Nutlin 3a for 24 h, then stained with antibodies against p53 (red) or actin (green) and DNA was counterstained with DAPI (blue). **(E)** Absence of a cell cycle arrest response in $p53^{Y217C/Y217C}$ MEFs. Asynchronous cell populations of $p53^{+/+}$, $p53^{Y217C/Y217C}$ and $p53^{-/-}$ MEFs were analyzed 24 hr after 0, 3 or 12 Gy ɣ-irradiation. Results from 3 independent experiments. **(F)** Absence of a p53-dependent apoptotic response in $p53^{Y217C/Y217C}$ thymocytes. Age-matched mice of the indicated genotypes were left untreated or submitted to 10 Gy whole-body ɣ-irradiation then sacrificed after 4 hr and their thymocytes were stained with Annexin V-FITC and analyzed by FACS, in 2 independent experiments. ***P<0.001, **P<0.01, *P<0.05, °P=0.09, ns: non-significant by Student's t tests.

A

at weaning

$p53^{+/-}$ x $p53^{+/-}$	Nbr. females obs (exp)	Nbr. males obs (exp)	Sex ratio (f/m)	Total
$p53^{+/+}$	24 (25)	20 (25)	1.2	196
$p53^{+/-}$	59 (49)	57 (49)	1.04	
$p53^{-/-}$	8 (25)	28 (25)	0.29	

$p53^{+/YC}$ x $p53^{+/YC}$	Nbr. females obs (exp)	Nbr. males obs (exp)	Sex ratio (f/m)	Total
$p53^{+/+}$	60 (67)	61 (67)	0.98	535
$p53^{+/YC}$	171 (134)	182 (134)	0.94	
$p53^{YC/YC}$	3 (67)	58 (67)	0.05	

B

E12.5-E16.5 embryos

$p53^{+/YC}$ x $p53^{+/YC}$ or $p53^{+/YC}$ x $p53^{YC/YC}$	Nbr. females	f exenc. (o.a.)	Nbr. males	m exenc. (o.a.)	Sex ratio (f/m)	Total
$p53^{+/+}$	12	0 (0)	14	0 (0)	0.86	169
$p53^{+/YC}$	47	0 (0)	48	0 (0)	0.98	
$p53^{YC/YC}$	26	10 (1)	22	0 (0)	1.18	

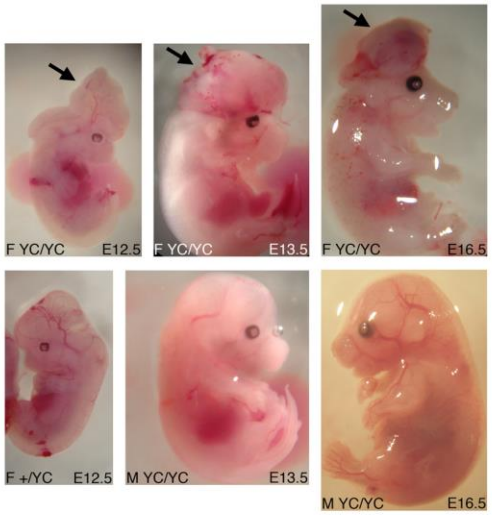

C

at birth

$p53^{+/YC}$ x $p53^{+/YC}$ or $p53^{+/YC}$ x $p53^{YC/YC}$	Nbr. females	Nbr. males	Sex ratio (f/m)	Total
$p53^{+/+}$	20	18	1.11	162
$p53^{+/YC}$	50	47	1.06	
$p53^{YC/YC}$	5	22	0.23	

Figure 3. $p53^{Y217C/Y217C}$ mice exhibit female-specific perinatal lethality.

(A) Distribution of weaned mice obtained from $p53^{+/-}$ or $p53^{+/Y217C}$ intercrosses. Obs: observed numbers of mice at weaning (P21); exp: expected numbers assuming a Mendelian distribution without sex distortion; f/m: observed female/male ratios. Consistent with previous reports the observed distribution of weaned mice from $p53^{+/-}$ intercrosses did not conform to values expected for a Mendelian distribution without sex distortion (υ=5; χ^2= 16.3>15.09), indicating a significant deficit in female $p53^{-/-}$ mice (top). The distribution of weaned mice from $p53^{+/Y217C}$ intercrosses diverged even more from values for a Mendelian distribution without sex distortion

(υ =5; χ^2= 91.02>15.09), due to a striking deficit in female $p53^{Y217C/Y217C}$ mice (bottom). The female frequency is significantly lower for $p53^{Y217C/Y217C}$ (3/535) than for $p53^{-/-}$ (8/196) females (P=0.0018 in a Fischer's test). **(B)** Exencephaly is frequently observed in $p53^{Y217C/Y217C}$ female embryos. Top: the distribution of E12.5-16.5 embryos from heterozygous ($p53^{+/Y217C}$) intercrosses or heterozygous-homozygous ($p53^{+/Y217C}$ x $p53^{Y217C/Y217C}$) crosses is shown. f or m exenc.: number of female or male embryos with exencephaly; o.a.: embryos with other abnormalities. Below, examples of female $p53^{Y217C/Y217C}$ embryos at E12.5, 13.5 and 16.5 exhibiting exencephaly (arrows) are each shown (center) together with a normal embryo from the same litter (bottom). **(C)** Distribution of mice at birth from the indicated crosses.

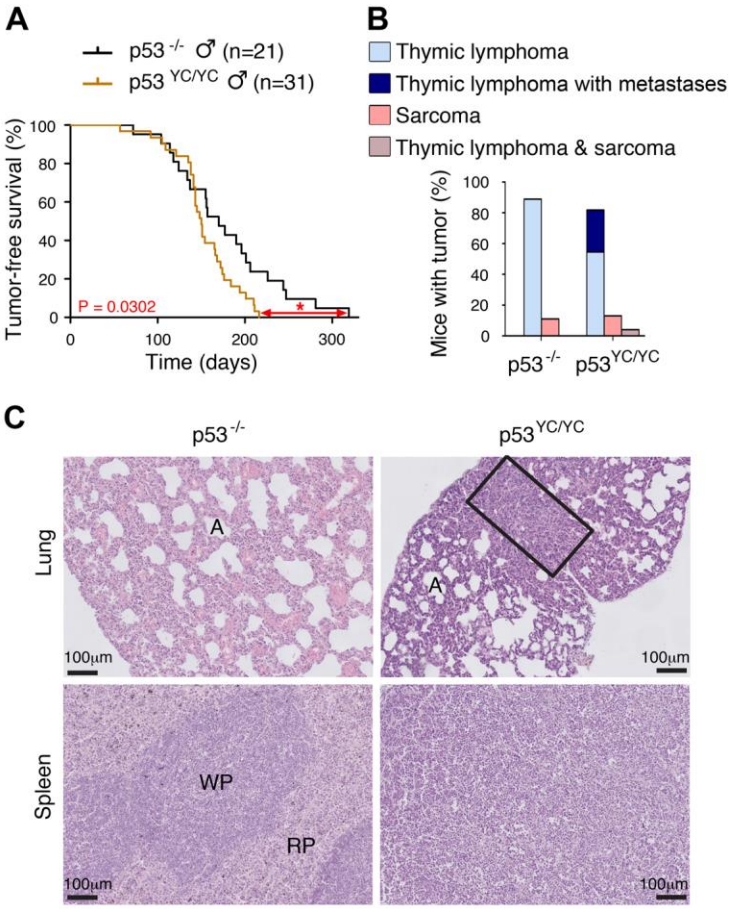

Figure 4. Oncogenic effects of the mutant protein in p53$^{Y217C/Y217C}$ male mice.
(A-B) In homozygous males, p53^{Y217C} leads to accelerated tumor onset and death (A), and aggressive metastatic tumors (B); n=cohort size. **(C)** Hematoxylin and eosin (H&E) staining of sections from the lung (top) and spleen (bottom) of p53$^{-/-}$ and p53$^{Y217C/Y217C}$ male mice, showing metastases in p53$^{Y217C/Y217C}$ animals. Normal organ structures are shown, with "A" indicating pulmonary alveoli, and "WP" and "RP" standing for splenic white and red pulp, respectively. In the lung section of the p53$^{Y217C/Y217C}$ mouse, the rectangle indicates a lymphoma area. In the spleen section of the p53$^{Y217C/Y217C}$ mouse, the typical splenic structures are absent due to massive tissue homogenization of the spleen by lymphoma cells.

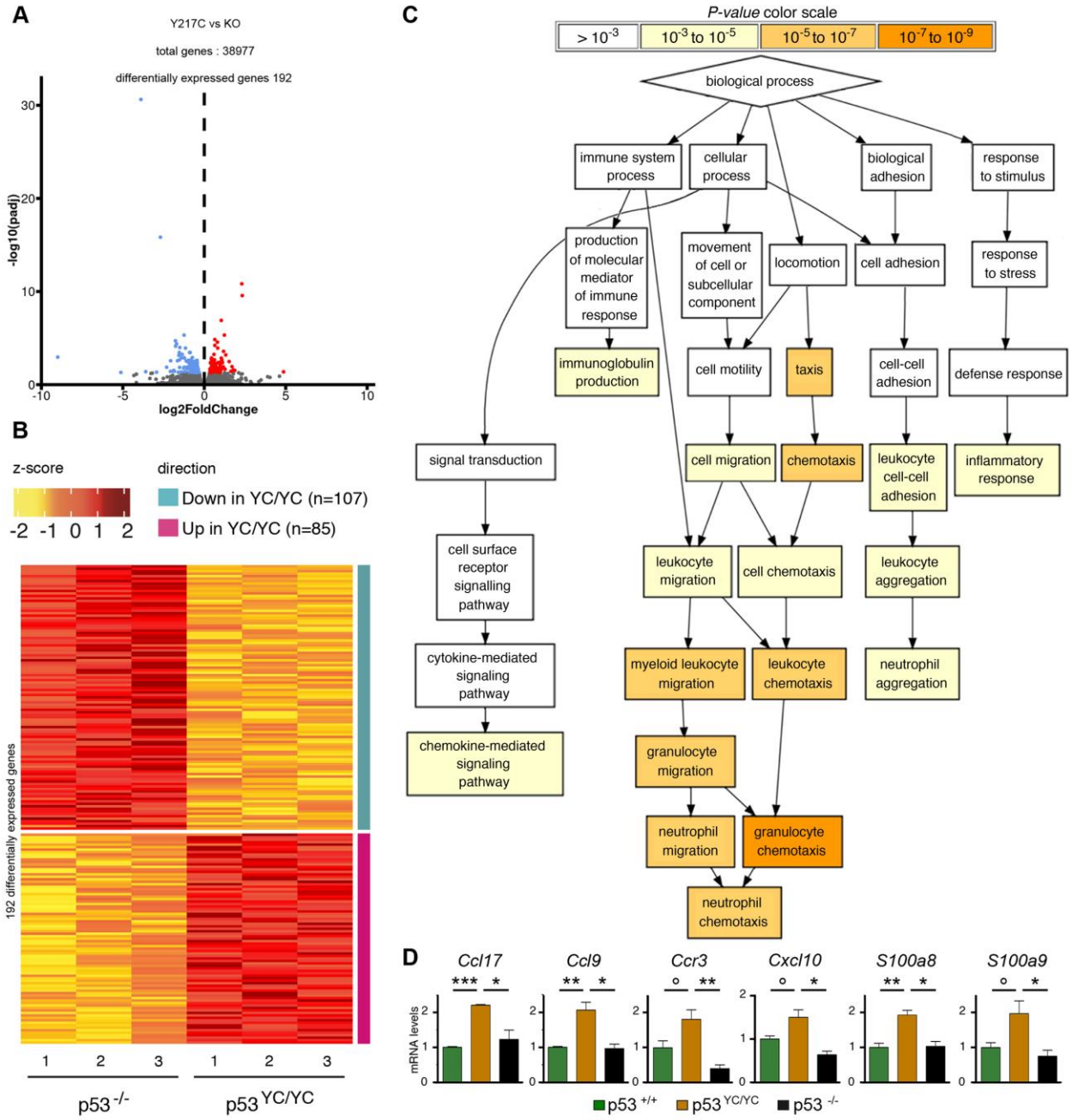

E

GENE SET NAME	NES	NOM p-val	FDR q-val
WP_ELECTRON_TRANSPORT_CHAIN	2.3558052	0.0	0.0
REACTOME_ANTIMICROBIAL_PEPTIDES	2.2443378	0.0	0.0
REACTOME_TRANSLATION	2.2320845	0.0	0.0
REACTOME_RESPIRATORY_ELECTRON_TRANSPORT_ATP_SYNTHESIS_BY_CHEMIOSMOTIC_COUPLING _AND_HEAT_PRODUCTION_BY_UNCOUPLING_PROTEINS	2.1794727	0.0	4.955357E-4
REACTOME_MITOCHONDRIAL_TRANSLATION	2.1783278	0.0	3.9642857E-4
REACTOME_DEPOSITION_OF_NEW_CENPA_CONTAINING_NUCLEOSOMES_AT_THE_CENTROMERE	2.1476152	0.0	0.0016925472
REACTOME_RMTS_METHYLATE_HISTONE_ARGININES	2.1314094	0.0	0.00187209
REACTOME_RESPIRATORY_ELECTRON_TRANSPORT	2.1104455	0.0	0.0021443255
REACTOME_PRC2_METHYLATES_HISTONES_AND_DNA	2.103474	0.0	0.0021457656
REACTOME_CHEMOKINE_RECEPTORS_BIND_CHEMOKINES	2.0778365	0.0	0.0028372295
REACTOME_DEFENSINS	2.0432084	0.0	0.0038559462
REACTOME_EUKARYOTIC_TRANSLATION_INITIATION	2.0400345	0.0	0.0036215642
WP_OXIDATIVE_PHOSPHORYLATION	2.0248396	0.0	0.0049684355

Figure 5. Increased expression of genes associated with white blood cell chemotaxis and inflammation in p53$^{Y217C/Y217C}$ male thymi.

(A-B) RNAseq analysis of thymi from p53$^{Y217C/Y217C}$ (n=3) and p53$^{-/-}$ (n=3) 8 weeks-old male mice. Volcano plot (A), with differentially expressed genes (DEGs), downregulated (blue) or upregulated (red) in p53$^{Y217C/Y217C}$ cells. Unsupervised clustering heat-map plot (B), with 192 DEGs ranked according to $\log_2$ fold changes. **(C)** Gene Ontology (GO) analysis of DEGs. Out of 192 DEGs, 141 are associated with at least one GO term, according to the Gene Ontology enRIchment anaLysis and visuaLizAtion tool (GOrilla). For each GO term, enrichment was calculated by comparing with the full list of 19759 genes associated with a GO term, and results are presented here with a color scale according to P-value of enrichment. This analysis mainly revealed an enrichment for genes associated with white blood cell chemotaxis/migration and inflammation, as shown here. Complete results of the analysis are presented in Figure S9. **(D)** RT-qPCR analysis of the indicated genes in thymi from 8 weeks-old p53$^{+/+}$, p53$^{Y217C/Y217C}$ and p53$^{-/-}$ male mice. Means + s.e.m. (n=3 per genotype). ***P<0.001, **P<0.01, *P<0.05, °P<0.075 by Student's t tests. **(E)** Gene set enrichment analysis (GSEA) of transcriptomes from p53$^{Y217C/Y217C}$ and p53$^{-/-}$ thymic cells. GSEA identified 13 gene sets enriched in p53$^{Y217C/Y217C}$ cells, with normalized enrichment scores (NES) > 2. Nominal p-values (NOM p-val) and false discovery rate q-values (FDR q-val) are indicated.

Supplemental Figures

Mouse 208- **T F R H S V V V P** Y **E P P E** A **G S** E Y **T T**- 228

Human 211- **T F R H S V V V P** Y **E P P E** V **G S** D C **T T**- 231

Figure S1. Protein sequence alignments showing homology between mouse p53 Tyrosine 217 and human p53 Tyrosine 220.
Portions of the DNA binding domains from the mouse (residues 208-228) and human (residues 211-231) p53 proteins are shown, with identical residues in bold, and mouse Tyrosine 217 and human Tyrosine 220 in red.

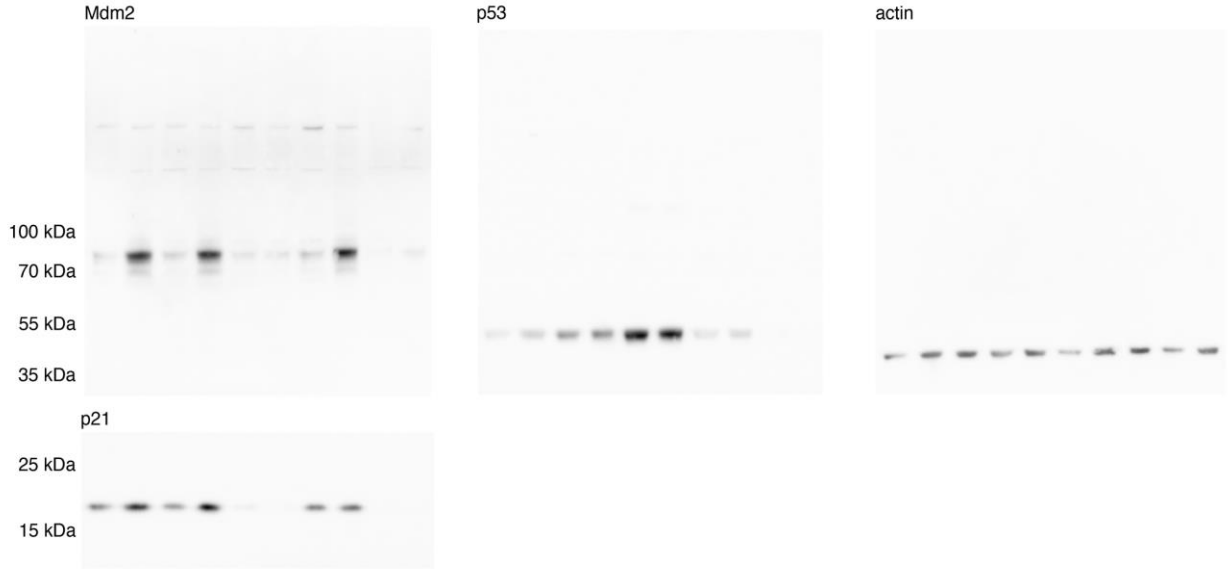

Figure S2. Uncropped images of the western blot presented in Figure 2A.
All images are from the same blot, cut in two below the 35KDa marker before incubation with the indicated antibodies.

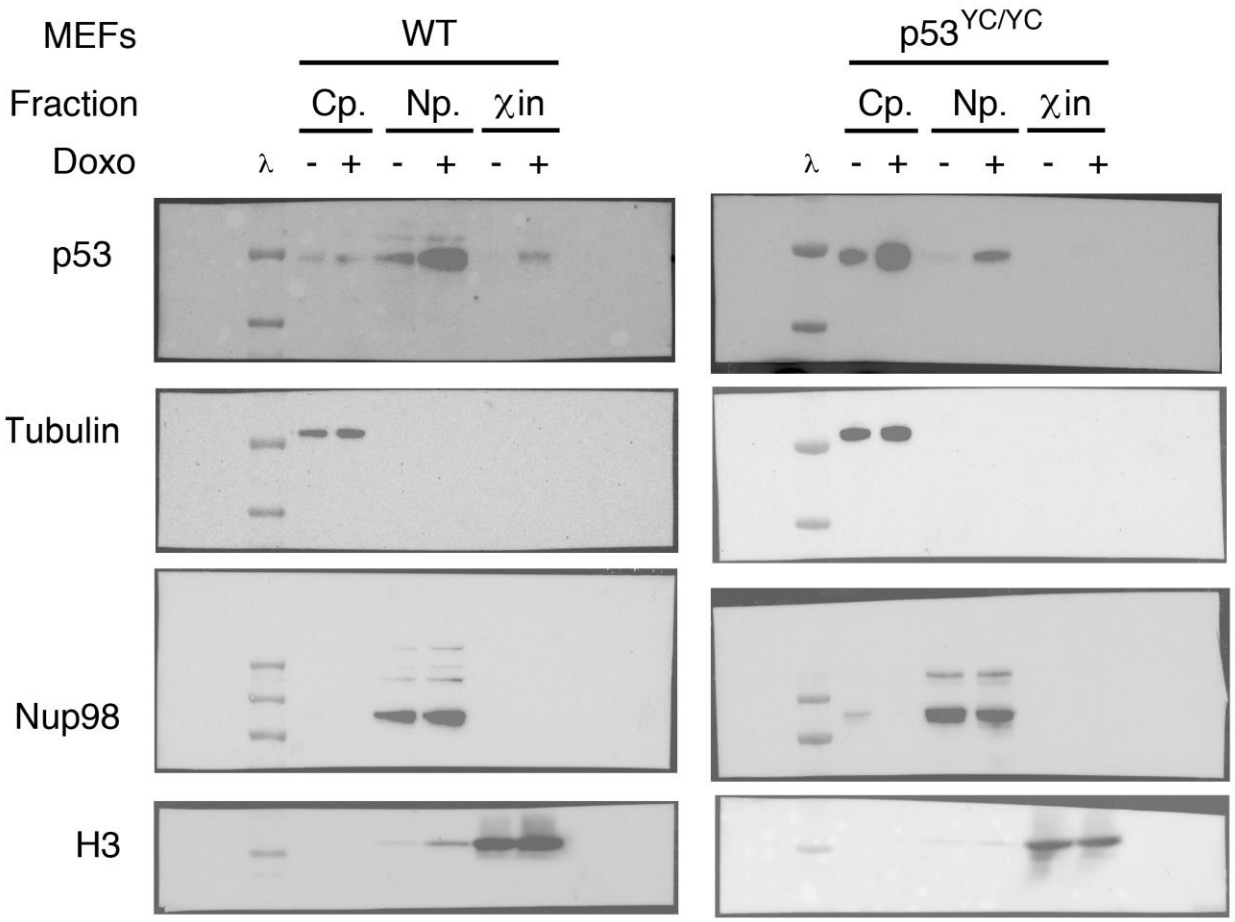

Figure S3. Uncropped images of the fractionation assays presented in Figure 2C. Chemiluminescence and colorimetric scans obtained with a ChemiDoc imaging system (Bio-Rad) were superposed to show the entire membranes, ladder lanes (λ), and chemiluminescence signals from subcellular fractions.

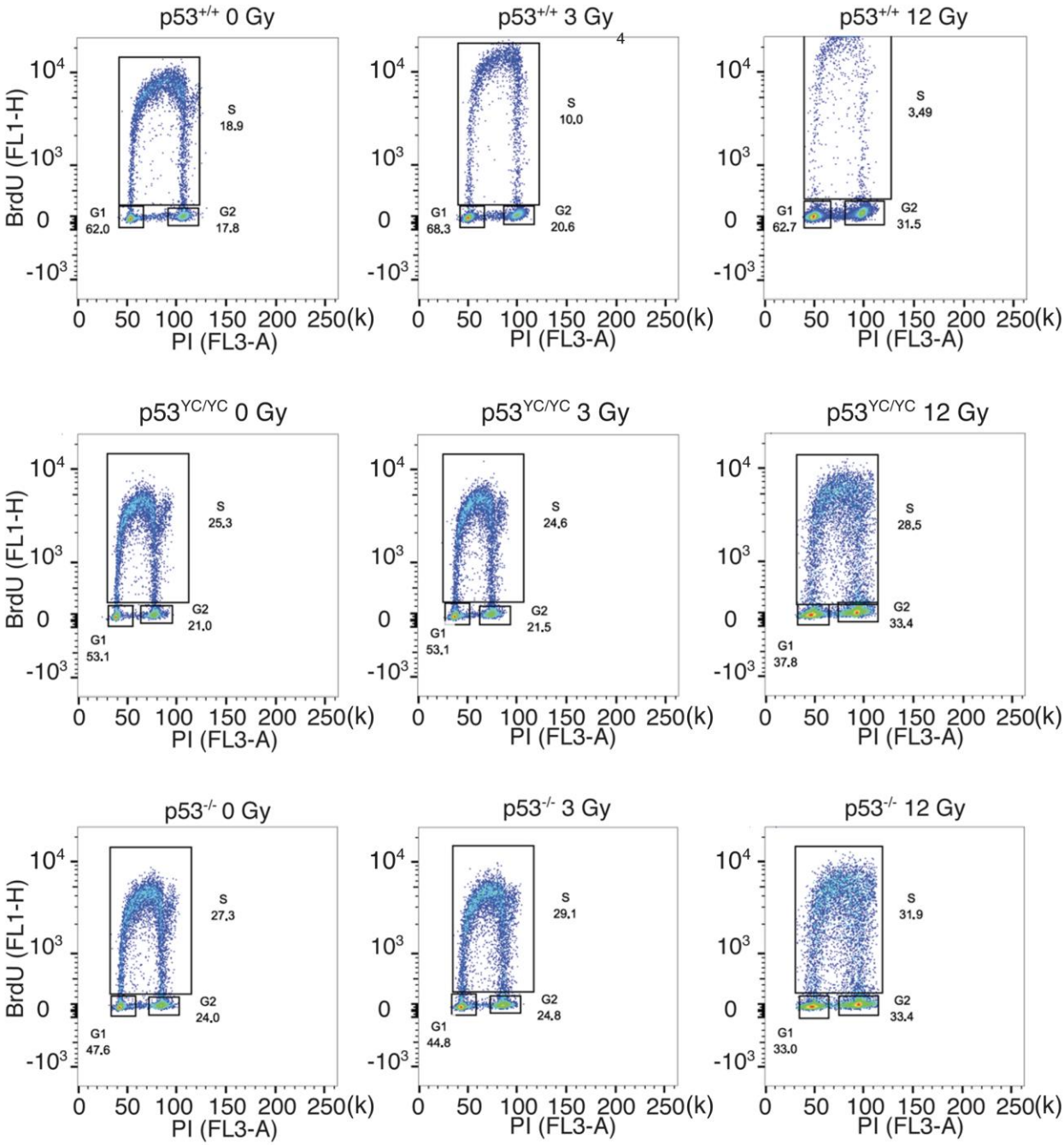

Figure S4. Cell cycle arrest responses of $p53^{+/+}$, $p53^{Y217C/Y217C}$ and $p53^{-/-}$ mouse embryonic fibroblasts.

Asynchronous MEFs were exposed to 0-12 Gy ɣ-irradiation, then after 24 hr cells were labelled with BrdU for 1 hr and analyzed by FACS. A typical experiment for cells of each genotype and condition is shown, with % cells in G1, S or G2/M mentioned in each panel.

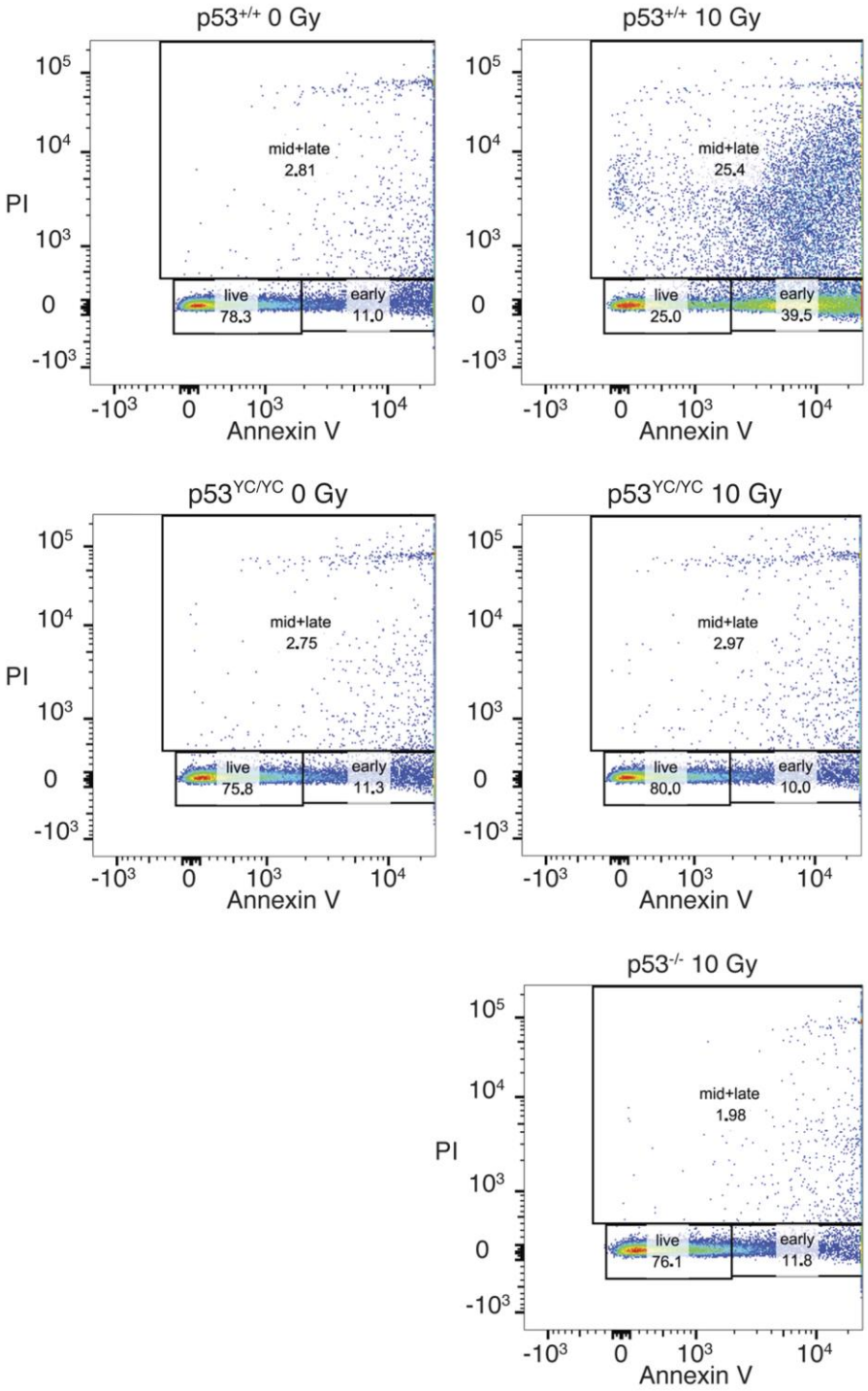

Figure S5. Apoptotic responses of $p53^{+/+}$, $p53^{-/-}$ and $p53^{Y217C/Y217C}$ thymocytes.
Mice were ɣ-irradiated (or not) and their thymocytes were recovered and analyzed by FACS after annexin V-FITC staining. A typical experiment for cells of each genotype and condition is shown. Numbers indicate % cells either alive (live), early apoptotic (early) or mid to late apoptotic (mid+late).

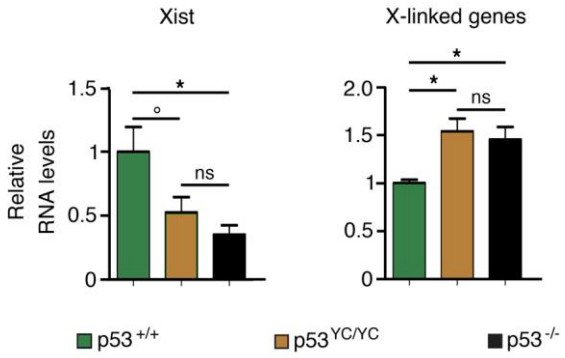

Figure S6. Evidence of aberrant chromosome X inactivation in p53$^{Y217C/Y217C}$ and p53$^{-/-}$ female embryos.

The expression of *Xist* and 3 X-linked genes (*Maob*, *Usp9x* and *Pls3*) was quantified in neurospheres from 2 p53$^{+/+}$, 5 p53$^{Y217C/Y217C}$ and 3 p53$^{-/-}$ female embryos by using real-time PCR, with results normalized to control mRNAs and mean RNA amounts in WT neurospheres assigned a value of 1. *P<0.05, °P=0.09, ns: non-significant by Student's t tests.

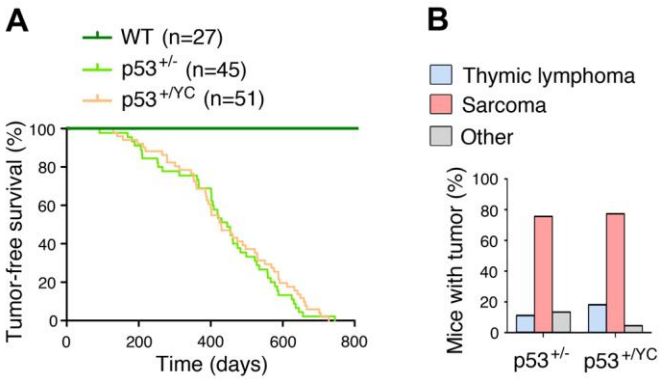

Figure S7. p53$^{+/Y217C}$ and p53$^{+/-}$ mice exhibit similar tumor onset and spectra.
No significant difference was observed between heterozygous p53$^{+/-}$ and p53$^{+/Y217C}$ mice, neither in spontaneous tumor onset and survival **(A)**, nor in tumor spectra **(B)**; n=cohort size. Mice of both sexes were included in this study.

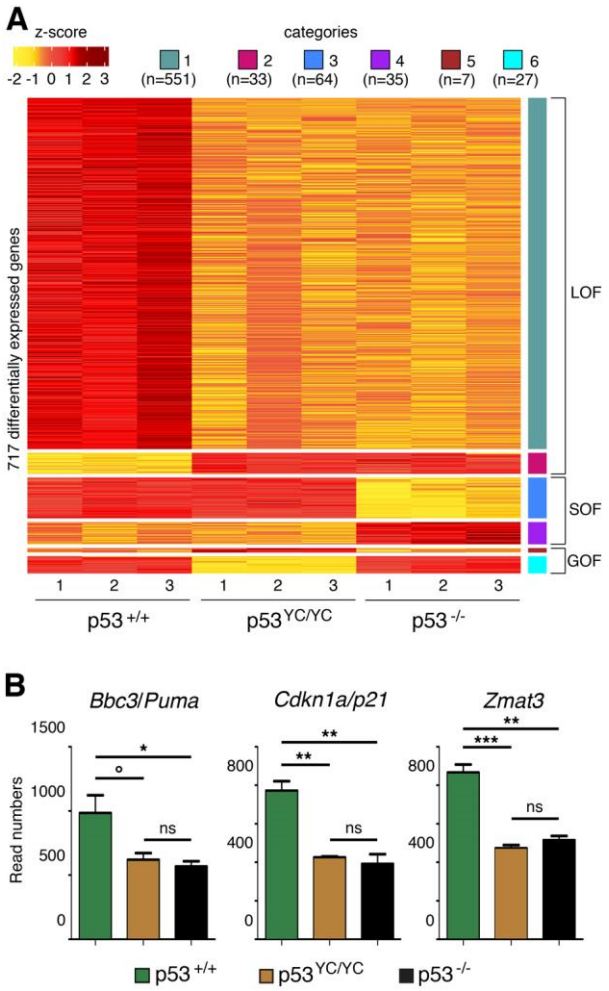

Figure S8. RNA-seq analysis from the thymi of 8 weeks-old p53$^{+/+}$, p53$^{Y217C/Y217C}$ and p53$^{-/-}$ male mice.

(A) Heat-Map plot, with 717 differentially expressed genes suggestive of a loss of function (LOF), a separation of function (SOF) or a gain of function (GOF) for the p53^{Y217C} mutant, ranked according to $\log_2$ fold change (n=number of genes). **(B)** Evidence of LOF in p53$^{Y217C/Y217C}$ cells for genes encoding Puma, p21 and Zmat3. Data from 3 mice per genotype. ***P<0.001, **P<0.01, *P<0.05, °P=0.07, ns: non-significant by Student's t tests.

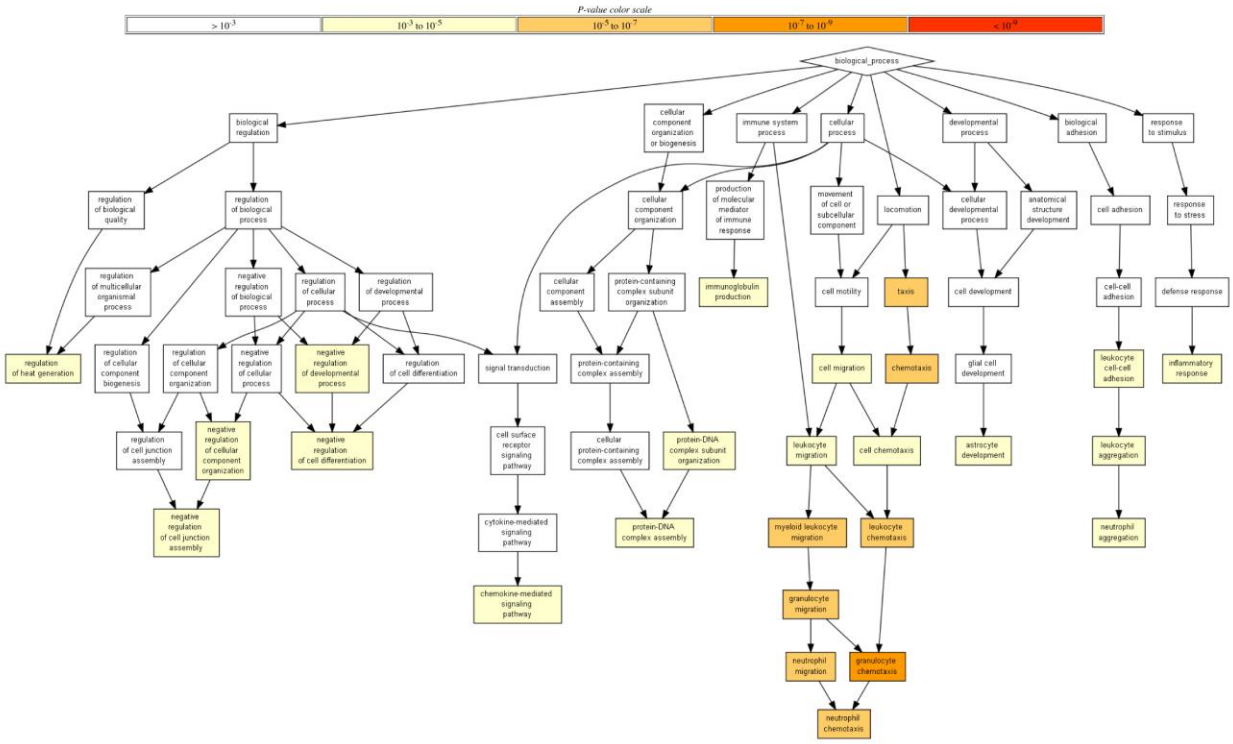

GO term	Description	P-value	FDR q-value	Enrichment (N, B, n, b)
GO:0071621	granulocyte chemotaxis	9.38E-8	1.45E-3	14.19 (19759,79,141,8)
GO:0097530	granulocyte migration	3.66E-7	2.82E-3	11.93 (19759,94,141,8)
GO:0030593	neutrophil chemotaxis	8.12E-7	4.18E-3	13.62 (19759,72,141,7)
GO:0006935	chemotaxis	1.51E-6	5.83E-3	5.66 (19759,297,141,12)
GO:0042330	taxis	1.8E-6	5.55E-3	5.57 (19759,302,141,12)
GO:0097529	myeloid leukocyte migration	2.08E-6	5.35E-3	9.50 (19759,118,141,8)
GO:1990266	neutrophil migration	2.14E-6	4.72E-3	11.82 (19759,83,141,7)
GO:0030595	leukocyte chemotaxis	3.61E-6	6.97E-3	8.83 (19759,127,141,8)
GO:0060326	cell chemotaxis	1.22E-5	2.09E-2	6.40 (19759,197,141,9)
GO:0006954	inflammatory response	4.68E-5	7.23E-2	4.02 (19759,418,141,12)
GO:0050900	leukocyte migration	8.05E-5	1.13E-1	5.75 (19759,195,141,8)
GO:0051129	negative regulation of cellular component organization	1.21E-4	1.55E-1	2.92 (19759,768,141,16)
GO:0070488	neutrophil aggregation	1.51E-4	1.79E-1	93.42 (19759,3,141,2)
GO:0070486	leukocyte aggregation	1.52E-4	1.68E-1	28.03 (19759,15,141,3)
GO:0031650	regulation of heat generation	1.86E-4	1.91E-1	26.28 (19759,16,141,3)
GO:0014002	astrocyte development	3.71E-4	3.58E-1	21.02 (19759,20,141,3)
GO:0071824	protein-DNA complex subunit organization	4.19E-4	3.81E-1	6.23 (19759,135,141,6)
GO:0045596	negative regulation of cell differentiation	4.71E-4	4.04E-1	2.69 (19759,781,141,15)
GO:0002377	immunoglobulin production	4.9E-4	3.98E-1	6.05 (19759,139,141,6)
GO:0070098	chemokine-mediated signaling pathway	5.55E-4	4.28E-1	10.58 (19759,53,141,4)
GO:1901889	negative regulation of cell junction assembly	5.67E-4	4.17E-1	18.28 (19759,23,141,3)
GO:0051093	negative regulation of developmental process	5.77E-4	4.05E-1	2.37 (19759,1064,141,18)
GO:0065004	protein-DNA complex assembly	5.97E-4	4E-1	7.38 (19759,95,141,5)
GO:0007159	leukocyte cell-cell adhesion	6.84E-4	4.4E-1	10.01 (19759,56,141,4)
GO:0016477	cell migration	9.44E-4	5.83E-1	2.51 (19759,836,141,15)

Species used: Mus musculus

The system has recognized 25139 genes out of 30795 gene terms entered by the user.
25081 genes were recognized by gene symbol and 58 genes by other gene IDs .
239 duplicate genes were removed (keeping the highest ranking instance of each gene) leaving a total of 24900 genes.
Only 19759 of these genes are associated with a GO term.

'**P-value**' is the enrichment p-value computed according to the mHG or HG model. This p-value is not corrected for multiple testing of 15431 GO terms.

'**FDR q-value**' is the correction of the above p-value for multiple testing using the Benjamini and Hochberg (1995) method.
Namely, for the ith term (ranked according to p-value) the FDR q-value is (p-value * number of GO terms) / i.

Enrichment (N, B, n, b) is defined as follows:
N - is the total number of genes
B - is the total number of genes associated with a specific GO term
n - is the number of genes in the target set when appropriate
b - is the number of genes in the intersection
Enrichment = (b/n) / (B/N)

Figure S9. Gene ontology analysis of differentially expressed genes.
The 192 differentially expressed genes (DEGs) between $p53^{-/-}$ and $p53^{Y217C/Y217C}$ thymocytes were analyzed with the Gene Ontology enRIchment anaLysis and visuaLizAtion tool (GOrilla). Out of 192 genes, 141 were associated with a GO term. For each GO term, enrichment was calculated by comparing with the full list of 19759 genes associated with a GO term. For example, genes with GO term #0071621 (granulocyte chemotaxis) represent 79/19759 genes associated with a GO term, but 8/141 of the identified DEGs, which represents a 14.19-fold enrichment.

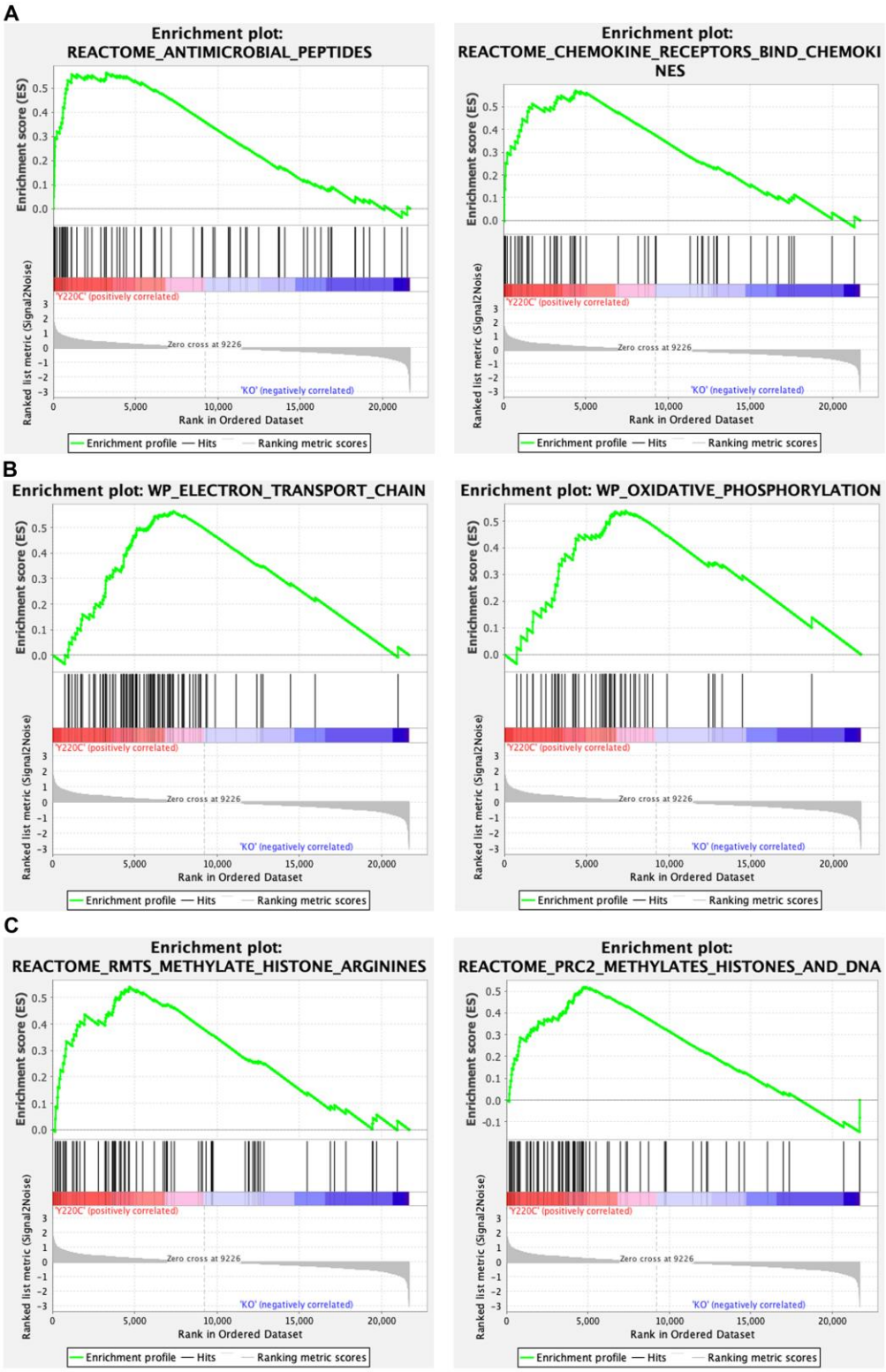

Figure S10. Gene set enrichment analysis (GSEA) of transcriptomes from p53$^{Y217C/Y217C}$ and p53$^{-/-}$ thymic cells: examples of GSEA enrichment plots.

Examples of GSEA enrichment plots indicating differences in immune responses **(A)**, mitochondrial function **(B)** and chromatin plasticity **(C)** are shown.

at weaning

$Mdm4^{+/-}$ $p53^{YC/YC}$ x $Mdm4^{+/-}$ $p53^{+/YC}$	**Nbr. females**	**Nbr. males**	**Sex ratio (f/m)**	**Total**
$Mdm4^{+/+}$ $p53^{+/YC}$	8	11	0.73	88
$Mdm4^{+/+}$ $p53^{YC/YC}$	0	9	0.00	
$Mdm4^{+/-}$ $p53^{+/YC}$	15	19	0.79	
$Mdm4^{+/-}$ $p53^{YC/YC}$	4	15	0.27	
$Mdm4^{-/-}$ $p53^{+/YC}$	0	0	NA	
$Mdm4^{-/-}$ $p53^{YC/YC}$	1	6	0.17	

$Mdm2^{+/-}$ $p53^{YC/YC}$ x $Mdm2^{+/-}$ $p53^{+/YC}$ or **$Mdm2^{-/-}$ $p53^{YC/YC}$ x $Mdm2^{+/-}$ $p53^{+/YC}$**	**Nbr. females**	**Nbr. males**	**Sex ratio (f/m)**	**Total**
$Mdm2^{+/+}$ $p53^{+/YC}$	3	0	NA	61
$Mdm2^{+/+}$ $p53^{YC/YC}$	0	3	0.00	
$Mdm2^{+/-}$ $p53^{+/YC}$	16	15	1.07	
$Mdm2^{+/-}$ $p53^{YC/YC}$	1	11	0.09	
$Mdm2^{-/-}$ $p53^{+/YC}$	0	0	NA	
$Mdm2^{-/-}$ $p53^{YC/YC}$	1	11	0.09	

Table S1. Viability of Mdm2 or Mdm4 loss in a $p53^{Y217C/Y217C}$ background.
Mouse distributions from the indicated crosses were determined at weaning.

F p53Y217C/Y217C a

mated with M p53+/Y217C **litter 1**

1 pup born 23 days after mating was initiated, found dead (partially eaten)
24 hr later, mother is still in labor
48 hr later, another pup found dead in cage, the mother appeared in pain and was sacrificed

F p53Y217C/Y217C b

mated with M p53+/Y217C **litter 1**

2 pups born 24 days after mating was initiated: 1 found dead, 1 alive (F p53+/Y217C)
litter 2
4 pups, all alive (1 F p53+/Y217C, 3 M p53+/Y217C)
litter 3
After extended labor (24 hr) pup fragments were found in cage,
the mother in pain was sacrificed with pups still inside the womb

Table S2. Evidence of dystocia in pregnant p53Y217C/Y217C females.
Results of the mating of two (a and b) p53Y217C/Y217C females (F) with a p53+/Y217C male (M) are shown. Both females were rapidly pregnant after encountering a male, but had to be sacrificed due to extended labor and pain during their first (female a) or third (female b) delivery.

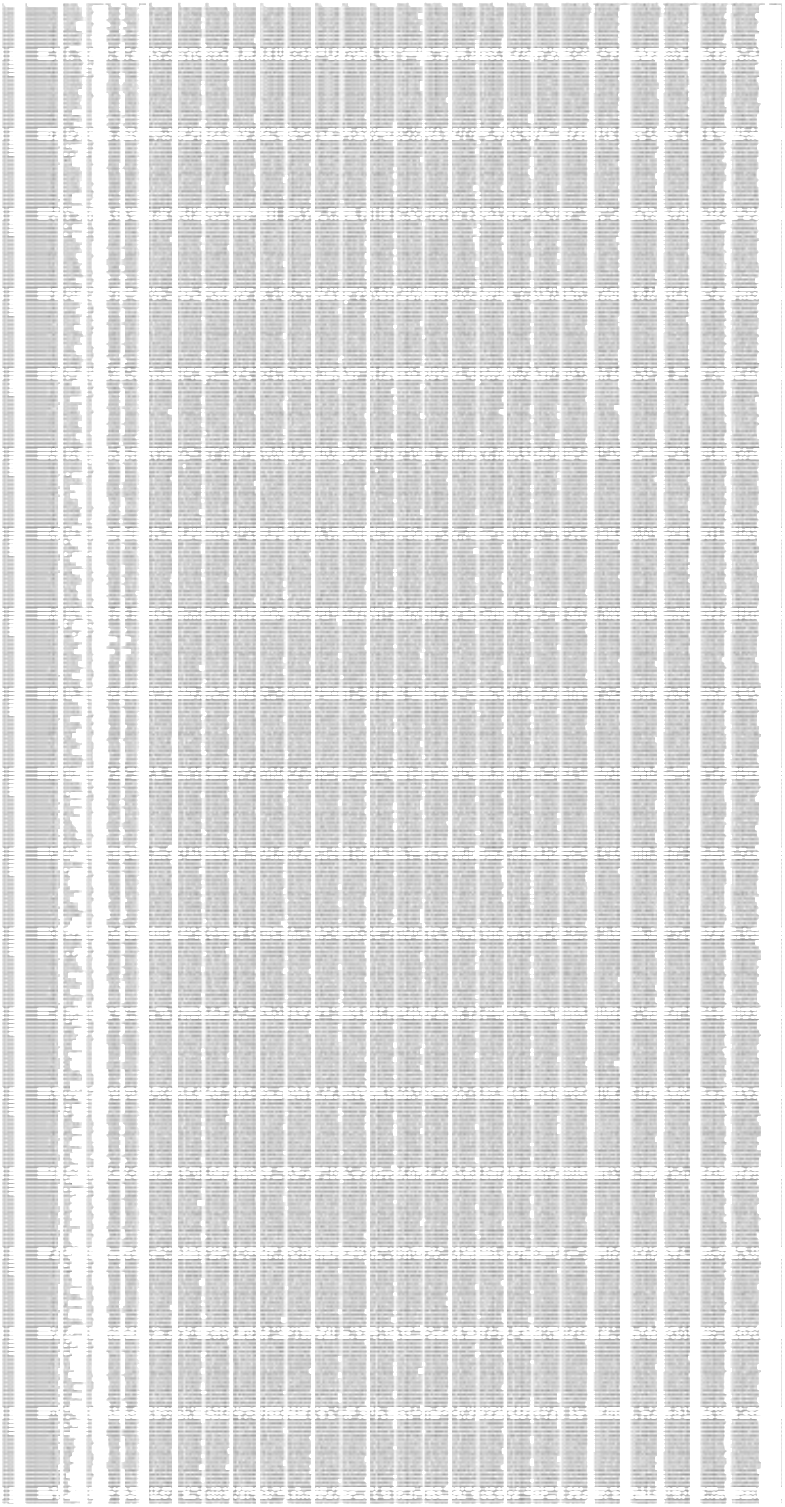

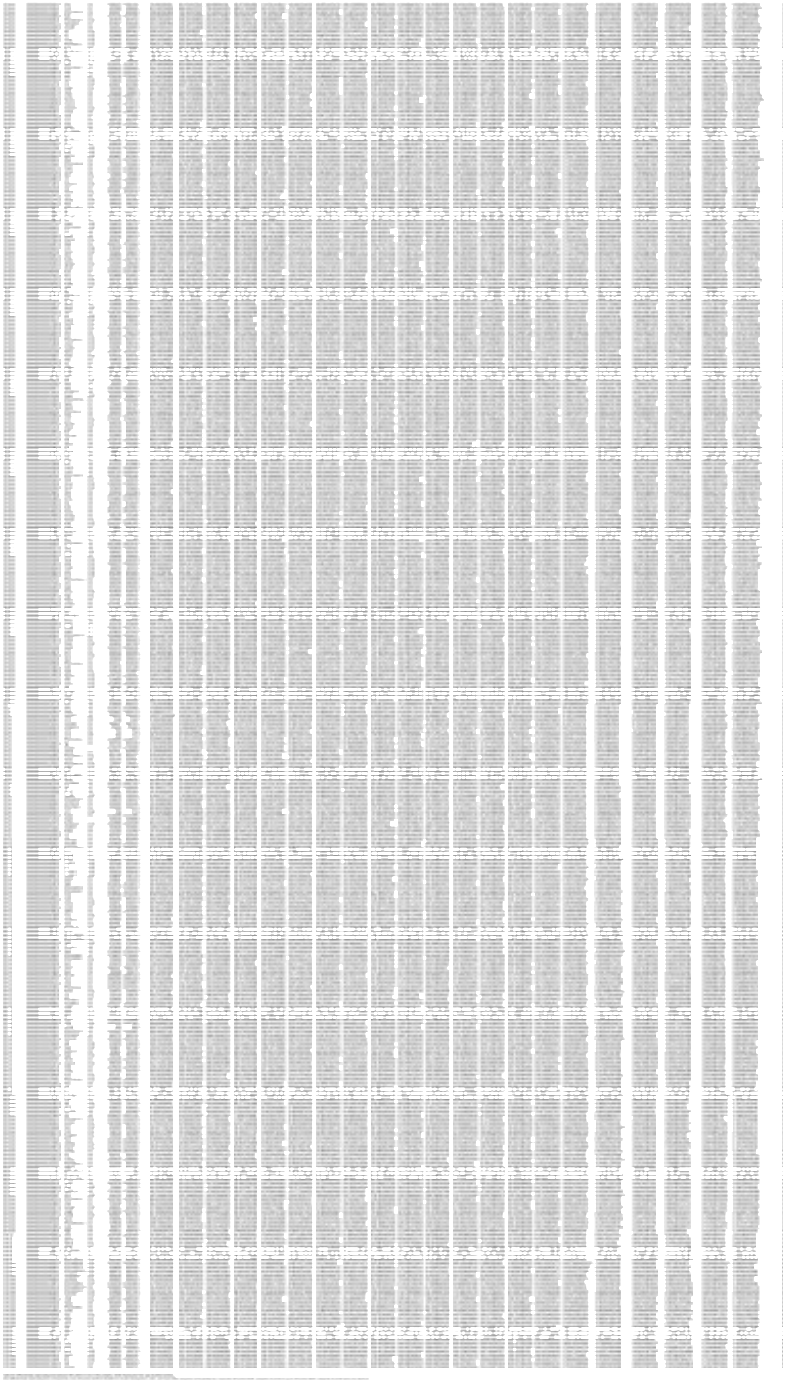

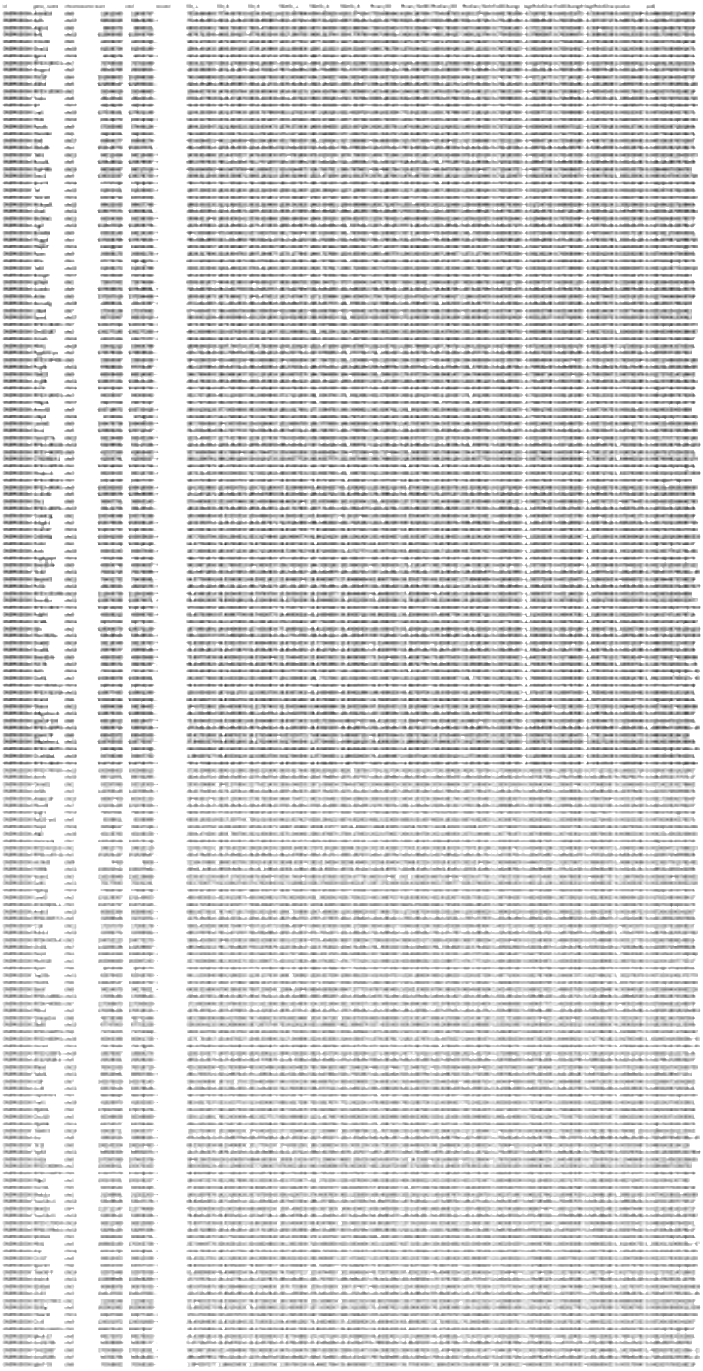

GO term	Description	*Ccl17*	*Ccl9*	*Ccr3*	*Cxcl10*	*S100a8*	*S100a9*
GO:0071621	granulocyte chemotaxis	x	x	x	x	x	x
GO:0097530	granulocyte migration	x	x	x	x	x	x
GO:0030593	neutrophil chemotaxis	x	x		x	x	x
GO:0006935	chemotaxis	x	x	x	x	x	x
GO:0042330	taxis	x	x	x	x	x	x
GO:0097529	myeloid leukocyte migration	x	x	x	x	x	x
GO:1990266	neutrophil migration	x	x		x	x	x
GO:0030595	leukocyte chemotaxis	x	x	x	x	x	x
GO:0060326	cell chemotaxis	x	x	x	x	x	x
GO:0006954	inflammatory response	x	x	x	x	x	x
GO:0050900	leukocyte migration	x	x	x	x	x	x
GO:0070488	neutrophil aggregation					x	x
GO:0070486	leukocyte aggregation					x	x
GO:0070098	chemokine-mediated signaling pathway	x	x		x		
GO:0007159	leukocyte cell-cell adhesion					x	x
GO:0016477	cell migration	x	x	x	x	x	x

Table S5. ***Ccl17*, *Ccl9*, *Ccr3*, *Cxcl10*, *S100a8* and *S100a9* are associated with GO terms of white blood cell migration/chemotaxis and inflammation.**

Locus	Forward Primer	Reverse Primer	Purpose
Trp53	GCGTAGTGGTACCTTGTGAGCCCCCCGAGGTCT	ACCTCGGGGGGCTCACAAGGTACCACTACGCTG	Mutagenesis (YC-F/R)
Trp53	CCTGGGAATACTTCAAGAGACG	CGTGATATTGCTGAAGAGCTTG	Genotyping (a, b)
Trp53	GTGTGTTGGCCATCTCTGTG	AACCGGACTCAGCGTCTCTA	Genotyping (c, d)
Ccl17	GCTGGTATAAGACCTCAGTGGAGTGT	GCTTGCCCTGGACAGTCAGA	qPCR
Ccl9	GCACAGCAAGGGCTTGAAA	CAGGCAGCAATCTGAAGAGTCTT	qPCR
Ccr3	CTGGACTCATAAAGGACTTAGCAAAA	TCTTGATTTCATCTGTGTTGAATGC	qPCR
Cdkn1a	GCAGACCAGCCTGACAGATTTC	TTCAGGGTTTTCTCTTGCAGAAG	qPCR
Cxcl10	AATGAAAGCGTTTAGCCAAAAAA	GGTGTGTGCGTGGCTTCAC	qPCR
Maob	GGTACAACCAGAATCATCTCAACAA	CTTGACCAGATCCACCAATAAATTT	qPCR
Mdm2	GTCTACCGAGGGTGCTGCAA	AAGCAATGGTTTTGGTCTAACCA	qPCR
Pls3	CCAGCACTAACTAAACCTGAAAACC	GGTTCTTTCTTCCCGAGTTTCC	qPCR
S100a8	TCCTTTGTCAGCTCCGTCTTC	GACGGCATTGTCACGAAAGAT	qPCR
S100a9	ACAAATGGTGGAAGCACAGTTG	TCATTTATGAGGGCTTCATTTCTCT	qPCR
Trp53	AAAGGATGCCCATGCTACAGA	TCTTGGTCTTCAGGTAGCTGGAG	qPCR
Usp9x	CTTGCTCAGCAGATTTCTGATGA	GCTGTAATCCTCCACATCCTGAT	qPCR
Ppia	TCTCCTTCGAGCTGTTTGCA	CAGTGCTCAGAGCTCGAAAGTTT	qPCR (control)
Rplp-0	CGACCTGGAAGTCCAACTAC	ATCTGCTGCATCTGCTTG	qPCR (control)
Cdkn1a	GTGAGGAGGAGCATGAATGGA	GGCAAAGTGGGACGTCCTTA	ChIP
Mdm2	CCGAGTTGACTCAGCTCTTCCT	ACCCCAGCTGGAGACATGTC	ChIP
Rbl2	CCAAGGGAAGCCACATGGT	ACCAGCCTTTCCATCTGCAT	ChIP (control)

Table S6. Primers used in this study.